J. Fluid Mech. (1982), *vol.* 125, *pp.* 283–317
Printed in Great Britain

Fluid dynamics and mass transfer in a gas centrifuge

By A. T. CONLISK,
Department of Mechanical Engineering, The Ohio State University, Columbus, OH

M. R. FOSTER
Department of Aeronautical and Astronautical Engineering, The Ohio State University, Columbus, OH

AND J. D. A. WALKER
Department of Mechanical Engineering and Mechanics, Lehigh University, Bethlehem, PA

(Received 4 August 1981 and in revised form 11 June 1982)

The fluid motion, temperature distribution and the mass-transfer problem of a binary gas mixture in a rapidly rotating centrifuge are investigated. The model centrifuge considered consists of a pair of concentric circular cylinders bounded on the top and bottom by horizontal end plates; the apparatus rotates rapidly about the axis of the cylinders. During steady operation a binary gas mixture containing species A and B is injected into and withdrawn from the centrifuge through axisymmetric slots located on the sidewalls. Solutions for the velocity, temperature and mass-fraction fields within the centrifuge are obtained for *mechanically* or *thermally* driven centrifuges. For the mass-transfer problem, a detailed analysis of the fluid-mechanical boundary layers is required, and, in particular, mass fluxes within the boundary layers are obtained for a wide range of source–sink geometries. Solutions to the mass-transfer problem are obtained for moderately and strongly forced flows in the container; the dependence of the separation (or enrichment) factor on centrifuge configuration, rotational speed and fraction of the volumetric flow rate extracted at the product port (the cut) are predicted.

1. Introduction

The mass-transfer or species-concentration problem in rapidly rotating containers has become an important research area in recent years because such problems often occur in industrial applications where separation of binary mixtures is required. Gas centrifuges are widely used to separate two-component mixtures by taking advantage of the large radial pressure gradient that is set up as a result of rapid rotation. The separation process is often called enrichment, since, for a binary mixture containing species A and B, the objective is to enrich the mixture in the desirable component species A, for example. Detailed experimentation is essentially impossible because of the high rotation rates that are typical of centrifuge operation (Olander 1972), and consequently it is important to develop a theoretical approach to such problems. The theoretical problem is made difficult because of the wide variety of complicated flows that can occur within a rapidly rotating centrifuge. Such flows have been the focus of a number of investigations since the original study of Sakurai & Matsuda (1974); in this latter study the motion of a gas within a circular cylindrical container, which rotates at large rates about the cylinder axis, was considered. The container walls were assumed to be perfectly thermally conducting and to be maintained at constant

temperature; motion within the container was induced by an applied thermal gradient between the horizontal endwalls of the container. Since the study of Sakurai & Matsuda (1974), a large number of investigations have been carried out, some of which are discussed by Soubbaramayer (1979), Conlisk (1978) and Bark & Hultgren (1979). In particular, the effects of various combinations of thermally insulating and thermally conducting walls for a wide variety of geometries have been considered by Matsuda, Hashimoto & Takeda (1976), Matsuda & Hashimoto (1978) and Matsuda & Takeda (1978). These studies are critically reviewed by Bark & Hultgren (1979), who also present a numerical method for the computation of the flow field and temperature distribution in geometries similar to those of the previous authors. In all of these studies, motion within the container geometry considered is driven by differential rotation of either a sidewall or an endwall, or by imposition of a temperature gradient across the container. In addition the containers were closed and there was no net mass transport through the apparatus.

However, centrifuges are normally operated continuously, whereby the binary mixture is continually injected and withdrawn from the rotating container during operation. The studies by Matsuda, Sukurai & Takeda (1975), Nakayama & Usui (1974) and Matsuda & Hashimoto (1976) do consider source–sink flows in combination with an applied thermal gradient. These investigations have been reviewed by Conlisk (1978), who points out that, for the most part, these studies do not convey a complete understanding of the flow field that exists in a typical centrifuge; this is because either the geometries considered were artificially selected in an attempt to avoid the presence of vertical shear layers or because the parameter ranges considered were not realistic. More recently, Wood & Morton (1980) have described an approximate method for the computation of the internal flow in a centrifuge with a source–sink flow.

In the present study, a model centrifuge is considered that is similar to the types discussed by Olander (1972). This model consists of a pair of concentric circular cylinders that are bounded in the vertical direction by horizontal end plates and that rotate rapidly about their common axis. A binary gas mixture is assumed to be continuously injected at some location on the inner radius through an axisymmetric slot; withdrawal of the separating mixture is assumed to take place at two or more locations on either the inner or outer radius through axisymmetric slots. The configuration is depicted schematically in cross-section in figure 1.

In the present study it will be demonstrated that the source–sink flow induces no vertical or significant radial motion within the geostrophic core region and that only an azimuthal velocity occurs in a direction opposite to the rotation. This swirl velocity is adjusted to relative rest on the solid walls through Ekman boundary layers on the horizontal end plates, and a set of vertical shear layers on the sidewalls; the entire mass transport due to the source–sink flow takes place through these boundary layers, as in the incompressible case (Hide 1968; Conlisk & Walker 1981). In this study, the mass-transfer problem for the binary gas mixture is considered, and it emerges that the separation process may be controlled and enhanced by inducing a vertical motion within the core region. A vertical velocity in the core region may be accomplished in at least two ways. In a thermally driven centrifuge (Olander 1972), a small temperature gradient is applied between the horizontal endwalls of the container; in a mechanically driven centrifuge one of the end plates is rotated at a slightly different rate than the rest of the container. In the present study, both effects as well as the source–sink flow are considered for a container having thermally conducting walls maintained at constant temperature.

The fluid-flow and heat-transfer problems for the model centrifuge are considered in §2 for a wide range of possible methods of injection into and withdrawal from the centrifuge. Solutions for the source–sink flow, as well as a variety of thermally induced and mechanically driven flows, are given for the geostropic flows. In addition, a detailed boundary-layer analysis is carried out in order to evaluate the mass fluxes in the boundary layers; these are required for consideration of the mass-transfer problem in §3.

In a gas centrifuge, the binary gas mixture is often injected from the inner cylinder into the annular region between the cylinders and the product gas, which is enriched in the desirable species (denoted here as species A) is withdrawn at some location, usually on the inner wall. The waste gas which is depleted in species A relative to the incoming mixture is normally withdrawn at some location on the periphery of the apparatus. It is worthwhile to note that this description of centrifuges is by no means universal and many other geometries have been studied as models for centrifuge applications (see e.g. Olander 1972; Matsuda *et al.* 1975; Nakayama & Usui 1974; Nakayama & Torii 1974); however, even for a given geometry the determination of where the entrance, product and waste ports should be located to achieve optimal performance is still an unsolved problem, principally because of the uncertainties that surround the proper method of solving the mass-transfer equation. As a first step toward resolving some of these difficulties, a particular source–sink configuration is adopted for the mass-transfer analysis. In addition, it is assumed that both species A and B in the binary mixture have large molecular weights, and further that species A is both the lighter species and the species for which enrichment is desired. In the model centrifuge depicted in figure 1, the binary gas enters the centrifuge through a small axisymmetric slot in the corner region of the bottom plate and inner cylinder. Gas is also extracted through a similar slot at the top plate on the inner axis; since gas near the axis is expected to be relatively lighter and therefore enriched in species A, this port is designated the product port in figure 1. The heavier species is expected to collect at the outer periphery; therefore gas is also extracted at a location on the outer cylinder at the bottom plate, and this axisymmetric slot is designated as the waste port.

The early theoretical work on the mass-transfer problem for the gas centrifuge and for heavy species is described in the review article by Olander (1972). In general, much of the early work suffers from a lack of knowledge of the nature of the velocity and temperature fields within the centrifuge. Often some approximate flow field was assumed; in many cases, the effects of either the endwalls or the sidewalls were neglected to produce 'long-bowl' and 'short-bowl' solutions respectively. Perhaps the most serious deficiency of this early work is that the importance of the fluid-mechanical boundary-layer structure to the mass-transfer problem was ignored. In the present study, it is demonstrated that the fluid-mechanical boundary layers have an important effect on the mass-transfer problem; furthermore, in one parameter range studied here, the species concentration itself exhibits a boundary-layer nature.

Several studies have appeared subsequent to the review of Olander (1972), but appear to suffer from the same types of deficiencies as the earlier work. Nakayama & Torii (1974) have considered a centrifuge configuration consisting of a cylindrical container in which gas is injected on the bottom plate through a small annular ring near the centre and product gas is withdrawn through an identical ring in the top plate; waste gas is withdrawn at the outer wall on the bottom plate and a refeed port is located on the top plate on the outer wall. A numerical solution to the mass-transfer equation was obtained using finite-difference methods and an impermeable wall

condition; the effects of thermal convection were neglected but subsequently incorporated in the study of Torii (1977). In both of these latter papers, the presence of the fluid-mechanical boundary layers and their influence on the mass-transfer problem was ignored. Sarma (1975) has considered the problem of mass transfer above an infinite rotating disk: however, this geometry is not closely related to the centrifuge. Matsuda (1975) has considered the solution of a radially averaged one-dimensional mass-transfer equation, but again without reference to the effects of the boundary layers. Brouwers (1976) has considered the effects on the fluid motion of aspect ratio in a rotating cylindrical container in which there are sources and sinks on the endwalls; the mass-transfer problem is briefly considered but the theoretical approaches described by Olander (1972) are used. Recent fluid-mechanical results and the latest work in the species-concentration problem have now been reviewed by Soubbaramayer (1979); however, no new approaches to the mass-transfer problem appear to have been undertaken.

An analysis of the mass-transfer problem requires the study of an additional equation that describes conservation of mass of one component of the binary mixture; the velocity and temperature fields appear as functions in this equation. In the analysis that is described in this paper, the solution to the mass-transfer equation for the species mass fraction $\omega_A = \rho_A^*/\rho^*$ will be considered for a wide range of physical parameters; here ρ^* and ρ_A^* are the total and species A density respectively. The plan of the mass-transfer analysis is as follows. In §3.1 a derivation of the mass-transfer equation is given; in §3.2 the mass-transfer boundary conditions are derived and the contribution due to the mass fluxes in the fluid-mechanical boundary layers is demonstrated. Three effects influence the mass-transfer process in a centrifuge. First, there is ordinary diffusion in which mass transfer occurs through a concentration gradient (Bird, Stewart & Lightfoot 1960, p. 503). Secondly, mass transfer is influenced by the bulk convective motion of the gas; finally, there is pressure diffusion in which mass transfer occurs owing to the large radial pressure gradient in the centrifuge. In §3.3, numerical solutions for the case where ordinary diffusion and convection are of comparable importance are described; an analytical solution for a convection-dominated problem is obtained in §3.4. Finally some general conclusions are given in §4.

2. Fluid mechanics and heat transfer

2.1. *Basic equations*

The basic centrifuge configuration considered in this study consists of an annular region bounded by horizontal end plates at $z^* = 0$ and $z^* = L$ and concentric circular cylinders at $r^* = aL$ and bL, where a and b are dimensionless and $a < b$. The apparatus is rapidly rotating with angular velocity $\boldsymbol{\Omega}$ about the axis of the cylinders, and a binary gas mixture is continuously injected into the container at some location on the inner radius and withdrawn at one more or more locations on the outer or inner wall; the walls are assumed to be maintained at constant but possibly different temperatures, and the upper and lower plates may be rotated at angular velocities slightly different from that of the vertical walls. A sketch of a cross-section of the model centrifuge is given in figure 1. In this study, the motions in the container induce changes in density and pressure that are small with respect to that of the binary gas mixture in solid-body rotation at constant temperature T_0^*. The equilibrium density and pressure distributions are governed by

$$\nabla^* p_e^* = -\rho_e^* \boldsymbol{\Omega}^2 \hat{\mathbf{k}} \times (\hat{\mathbf{k}} \times \mathbf{r}^*) - \rho_e^* g \hat{\mathbf{k}}, \tag{2.1}$$

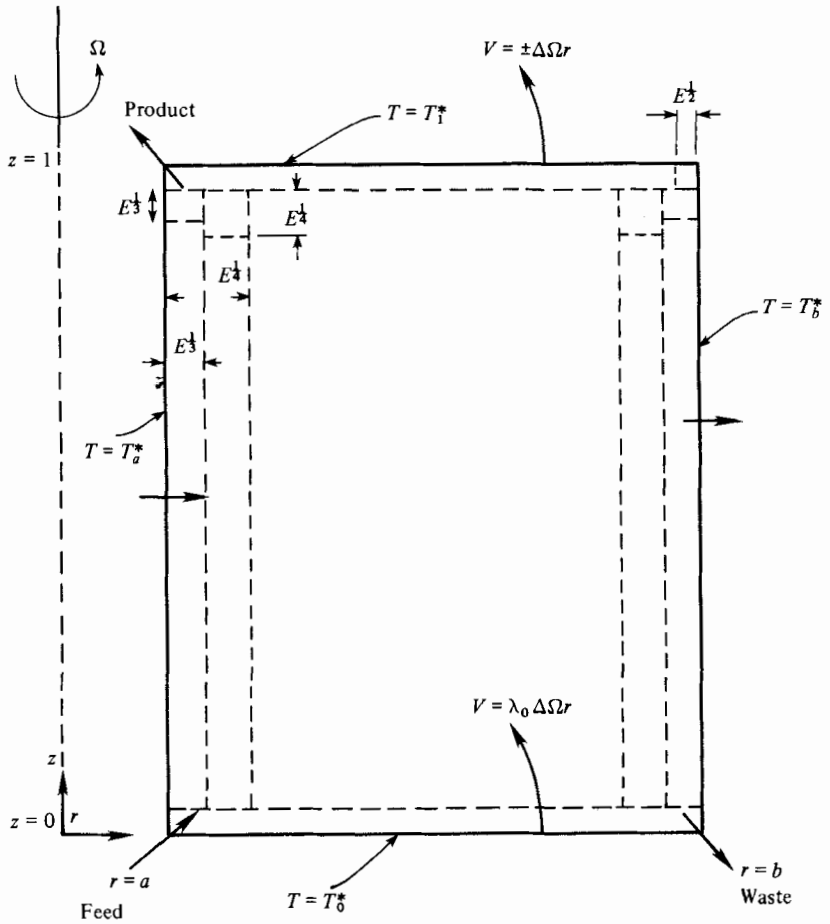

FIGURE 1. Geometry and coordinate system for a cross-section of the model centrifuge. Straight bold arrows indicate possible locations of injection or withdrawal. The container walls are at constant temperature and the top and bottom plates may be in differential rotation. Shear-layer structure is not to scale; note substructure near the upper corners for differential rotation of the top plate. The locations indicated product, feed and waste correspond to the particular source–sink geometry used in the mass-transfer analysis.

where g is the gravitational acceleration and $\hat{\mathbf{k}}$ is a unit vector perpendicular to the endwalls. Note that in general asterisks are used to denote dimensional quantities. The equation of state is taken to be the ideal-gas law, and, using $p_e^* = \rho_e^* RT_0^*$, the solution of (2.1) is

$$p_e^* = C^* \exp\{\tfrac{1}{2}M^2 r^2 - M^2 Fr\, z\}. \tag{2.2}$$

Here C^* is a constant and the dimensionless parameters appearing in (2.2) are the rotational Mach number M and the rotational Froude number Fr, defined by

$$M^2 = \frac{\Omega^2 L^2}{RT_0^*}, \quad Fr = \frac{g}{\Omega^2 L}. \tag{2.3}$$

In addition, $r = r^*/L$ and $z = z^*/L$ measure dimensionless distances in the radial and vertical directions respectively, and the gas constant $R = R_u/\overline{M}$, where R_u is the universal gas constant and $\overline{M}$ is the number-mean molecular weight of the mixture. The rotational Mach number is assumed to be $O(1)$.

In the present study, gravitational effects are assumed negligible in the sense that

$Fr \ll 1$†. A reference density ρ_0^* is defined corresponding to the mass density of the entering binary gas stream at the inner radius, and consequently the equilibrium pressure and density distributions, to leading order, are

$$p_e^* = \rho_0^* \rho_e(r)\, RT_0^*, \quad \rho_e^* = \rho_0^* \rho_e(r), \tag{2.4}$$

where

$$\rho_e(r) = \exp\{\tfrac{1}{2}M^2(r^2 - a^2)\}. \tag{2.5}$$

The net mass-flow rate through the container is assumed to be small and given by

$$\dot{m}^* = \dot{m}_0^* E^{\frac{1}{2}}, \tag{2.6}$$

where E is the Ekman number defined according to

$$E = \frac{\mu}{\rho_0^* \Omega L^2}, \tag{2.7}$$

with μ being the absolute viscosity. Typical values of E for modern centrifuges lie in the range 10^{-7}–10^{-9} (Soubbaramayer 1979). A representative velocity scale may be defined in terms of $\dot{m}_0^*$ according to

$$U_I = \frac{\dot{m}_0^*}{\rho_0^* L^2}, \tag{2.8}$$

and a fluid Rossby number ϵ_f is defined by

$$\epsilon_f = U_I / \Omega L. \tag{2.9}$$

The perturbations to the equilibrium pressure, density and temperature distributions arising from the imposed source–sink flow through the container are of relative order ϵ_f. Dimensionless perturbation quantities p, ρ, T are formally defined according to

$$p^* = p_e^*(1 + \epsilon_f p), \quad \rho^* = \rho_e^*(1 + \epsilon_f \rho), \quad T^* = T_0^*(1 + \epsilon_f T), \tag{2.10}$$

and to leading order the ideal gas equation becomes

$$p = \rho + T + O(\epsilon_f). \tag{2.11}$$

Note that in general μ is a function of pressure and temperature; however, one consequence of (2.10) is that the Ekman number as defined by (2.7) is constant to leading order.

Taking dimensionless cylindrical coordinates (r, θ, z) with origin on the axis of rotation on the bottom plate and with corresponding velocity components (u, v, w) (made dimensionless with respect to U_I), the equations governing the axisymmetric motion and temperature distribution are (to leading order)

$$\frac{\partial u}{\partial r} + \frac{u}{r} + \frac{\partial w}{\partial z} + rM^2 u = 0, \tag{2.12}$$

$$\epsilon_f\left\{u\frac{\partial u}{\partial r} + w\frac{\partial u}{\partial z} - \frac{v^2}{r} + \rho T\right\} - 2v = -rT - \frac{1}{M^2}\frac{\partial p}{\partial r} + \frac{E}{\rho_e(r)}\left\{\nabla^2 u - \frac{u}{r^2} - \frac{M^2}{3}\frac{\partial}{\partial r}(ru)\right\}, \tag{2.13}$$

$$\epsilon_f\left\{u\frac{\partial v}{\partial r} + w\frac{\partial v}{\partial z} + \frac{uv}{r}\right\} + 2u = \frac{E}{\rho_e(r)}\left\{\nabla^2 v - \frac{v}{r^2}\right\}, \tag{2.14}$$

$$\epsilon_f\left\{u\frac{\partial w}{\partial r} + w\frac{\partial w}{\partial z}\right\} = -\frac{1}{M^2}\frac{\partial p}{\partial z} + \frac{E}{\rho_e(r)}\left\{\nabla^2 w - \frac{M^2 r}{3}\frac{\partial u}{\partial z}\right\}, \tag{2.15}$$

$$\epsilon_f Pr\left\{u\frac{\partial T}{\partial r} + w\frac{\partial T}{\partial z}\right\} - 4hru = \frac{E}{\rho_e(r)}\nabla^2 T, \tag{2.16}$$

† Further analysis from §2.6 indicates the restriction is $Fr \ll E^{\frac{1}{4}}$.

where

$$h = \frac{\gamma - 1}{4\gamma} Pr\, M^2, \tag{2.17}$$

$$\nabla^2 = \frac{1}{r}\frac{\partial}{\partial r}\left(r\frac{\partial}{\partial r}\right) + \frac{\partial^2}{\partial z^2}. \tag{2.18}$$

Here Pr is the Prandtl number and γ is the ratio of specific heats, both of which are assumed to be constant to leading order. In (2.12) and in (2.13)–(2.16) the neglected terms are $O(\epsilon_f)$ and $O(\epsilon_f^2)$ respectively.

It is worthwhile to note that throughout this paper it is assumed that the ratio a of the inner radius to the centrifuge length and the ratio b of the outer radius to the length are $O(1)$ quantities. For a purely cylindrical centrifuge in which the feed flow is introduced through the end plates, the quantity b is normally termed the aspect ratio. Brouwers (1976) has considered the effect of different magnitudes of the aspect ratio for a cylindrical container, and finds that three types of flow can occur, corresponding to the parameter ranges $1 \gg b \gg E^{\frac{1}{4}}$, $E^{\frac{1}{3}} \gg b \sim E^{\frac{1}{4}}$ and $b \sim E^{\frac{1}{3}}$; the motion in the cylinder is driven either by sources and sinks on the endwalls, differential rotation of the end plates or by maintaining the sidewalls and endwalls at different temperatures. The geometry in Brouwers' (1976) study is different from the model centrifuge in the present study, but presumably similar methods could be used to investigate the modifications of the centrifuge dynamics in the present configuration for extreme aspect ratios.

The basic flow structure due to the source–sink flow is well known (Hide 1968) and consists of an interior geostrophic region, Ekman layers on the horizontal endwalls and a set of vertical shear layers on the sidewalls having thicknesses $O(E^{\frac{1}{3}})$ and $O(E^{\frac{1}{4}})$. In the present study, solutions are obtained on the basis of linear theory wherein the nonlinear terms on the left-hand side of (2.13)–(2.15) are neglected. It may be shown, using arguments similar to those of Bennetts & Hocking (1973) that, as ϵ_f is increased, the nonlinear terms in (2.13) and (2.15) first become important when $\epsilon_f = O(E^{\frac{1}{4}})$ and then in the $E^{\frac{1}{4}}$ layers; consequently the present analysis is valid in the parameter range $\epsilon_f \ll E^{\frac{1}{4}}$. One consequence of the linearity is that here the effects of three distinct types of fluid motion may be considered separately. The first of these motions results from the source–sink flow, and the appropriate boundary conditions for this problem are

$$u = v = w = T = 0 \tag{2.19}$$

on all solid walls except at a location of injection or withdrawal. It emerges that the radial and vertical velocities within the geostrophic core due to the imposed source–sink flow are very small; for this reason additional types of motion must be considered, since separation of the binary mixture is significantly affected by vertical motion within the geostrophic core region. In the centrifuge configuration considered in this study there are at least two ways in which significant vertical motion in the core region may be induced. In a thermally driven centrifuge, a small temperature gradient is imposed by heating the upper end plate to a temperature T_1^* above the reference temperature T_0^* of the lower horizontal plate. A thermal Rossby number may be defined according to

$$\epsilon_T = \frac{T_1^* - T_0^*}{T_0^*}, \tag{2.20}$$

and the thermal boundary conditions for the perturbation temperature become

$$T = 0 \quad \text{at} \quad z = 0, \quad T = \frac{\epsilon_T}{\epsilon_f} \quad \text{at} \quad z = 1. \tag{2.21}$$

If the imposed temperature gradient is such that $\epsilon_T \ll \epsilon_f$, the effects of the imposed temperature gradient are negligible to leading order; on the other hand, in the case of interest $\epsilon_T = O(\epsilon_f)$, and the effects of the source–sink flow and heat transfer are comparable. Defining $\epsilon_T = \lambda_T \epsilon_f$, (2.21) become

$$T = 0 \quad \text{at} \quad z = 0, \quad T = \lambda_T \quad \text{at} \quad z = 1. \tag{2.22}$$

Furthermore, if the sidewalls at $r = a$ and $r = b$ are maintained at constant temperatures T_a^* and T_b^*, the sidewall thermal conditions may be written

$$T = \lambda_a \lambda_T \quad \text{at} \quad r = a, \quad T = \lambda_b \lambda_T \quad \text{at} \quad r = b, \tag{2.23}$$

where $\lambda_a = (T_a^* - T_0^*)/(T_1^* - T_0^*)$ and the definition of λ_b is analogous.

The third effect considered here occurs in a mechanically driven centrifuge, where vertical motion within the core region is induced by a differential rotation of the end plates. A mechanical Rossby number ϵ_m may be defined according to

$$\epsilon_m = \Delta\Omega/\Omega, \tag{2.24}$$

where $\Delta\Omega$ is the magnitude of the differential rotation. Defining λ_m by

$$\lambda_m = \epsilon_m/\epsilon_f, \tag{2.25}$$

the effects of differential rotation are comparable to those of the imposed source-sink flow for $\lambda_m = O(1)$. For this problem, the boundary conditions for u, w and T are homogeneous, and on the end plates

$$v = \lambda_m \lambda_1 r \quad \text{at} \quad z = 1, \quad v = \lambda_m \lambda_0 r \quad \text{at} \quad z = 0. \tag{2.26}$$

Here $\lambda_1 = \pm 1$, and λ_0 is a constant, which may be either positive or negative.

2.2. *The geostrophic flow*

Within the geostrophic core, it follows from (2.12)–(2.16) that, in general, the leading terms in the expansions for the pressure, velocities and temperature are

$$u = EU_G(r, z) + \ldots, \quad v = V_G(r, z) + \ldots, \quad w = E^{\frac{1}{2}} W_G(r) + \ldots, \tag{2.27}$$

$$T = T_G(r, z) + \ldots, \quad p = P_G(r) + \ldots, \tag{2.28}$$

where the leading term in w is $O(E^{\frac{1}{2}})$ for compatibility with the Ekman layers on the horizontal plates. Ekman layers are required to adjust the azimuthal geostrophic velocity in (2.27) to the appropriate value on the horizontal boundary. It may be easily demonstrated (Barcilon 1970) that the nonlinear terms in (2.13)–(2.15) may be neglected provided that $\epsilon_f \ll 1$. Define a scaled Ekman-layer variable according to

$$\zeta = \sigma^{\frac{1}{4}} \left(\frac{\rho_e(r)}{E}\right)^{\frac{1}{2}} z, \quad \zeta = \sigma^{\frac{1}{4}} \left(\frac{\rho_e(r)}{E}\right)^{\frac{1}{2}} (1 - z), \tag{2.29}$$

on the bottom and top plates respectively, where

$$\sigma(r) = 1 + hr^2. \tag{2.30}$$

It may easily be shown (see e.g. Sakurai & Matsuda 1974), upon substitution in (2.13)–(2.16), that

$$\frac{\partial^2}{\partial \zeta^2}(T + 2hrv) = 0, \tag{2.31}$$

and consequently

$$T + 2hrv = T_G + 2hrV_G = T_B(r, z_0) + 2hrV_B(r, z_0). \tag{2.32}$$

The subscript B in general denotes that a quantity is evaluated on the boundary of the container; here $z_0 = 0$ or 1 and the right-hand side of (2.32) is evaluated on the lower or upper horizontal plate. The Ekman-layer solution for the radial and azimuthal velocities is conveniently expressed in terms of the complex variable $\chi = u + i\sigma^{\frac{1}{2}}v$, and it may be shown that

$$\chi = i\sigma^{\frac{1}{2}}V_G(r) + i\sigma^{\frac{1}{2}}\{V_B(r, z_0) - V_G(r)\}e^{-(1+i)\zeta}. \tag{2.33}$$

There are two important aspects of this solution. The first of these may be obtained by integration of (2.33) across the Ekman layer, and is that there is a dimensionless mass flux radially outward in each Ekman layer having a value of

$$\tfrac{1}{2}\sigma^{\frac{1}{4}}\{\rho_e(r)E\}^{\frac{1}{2}}\{V_B(r, z_0) - V_G(r, z_0)\} \tag{2.34}$$

per unit length of circumference. The second aspect is the Ekman compatibility condition

$$w = \pm\frac{E^{\frac{1}{2}}}{2r\rho_e(r)}\frac{\partial}{\partial r}\{r\sigma^{\frac{1}{4}}\rho_e^{\frac{1}{2}}\{v - V_B(r, z_0)\}\} \quad \text{at} \quad z_0 = \tfrac{1}{2} \mp \tfrac{1}{2}. \tag{2.35}$$

This relation is readily obtained through use of the continuity equation and integration across the Ekman layer to obtain the vertical velocity at the Ekman-layer edge.

At this stage it is useful to establish some general relations for the geostrophic flow. Since u is $O(E)$ and w is $O(E^{\frac{1}{2}})$ in the core, it follows from (2.13) that

$$V_G = \tfrac{1}{2}rT_G + P(r), \tag{2.36}$$

for $\epsilon_f \ll 1$, where

$$P(r) = \frac{1}{2M^2}\frac{dP_G}{dr}. \tag{2.37}$$

Equations (2.32) and (2.36) may be combined to eliminate T_G, and this gives

$$\sigma V_G(r, z_0) = \tfrac{1}{2}rT_B(r, z_0) + hr^2 V_B(r, z_0) + P(r). \tag{2.38}$$

Taking $z_0 = 0$ and 1 in (2.38) and adding the resulting two equations leads to

$$P(r) = \tfrac{1}{2}\sigma\{V_G(r,1) + V_G(r, 0)\} - \tfrac{1}{4}r\{T_B(r,1) + T_B(r, 0)\} - \tfrac{1}{2}hr^2\{V_B(r, 1) + V_B(r, 0)\}. \tag{2.39}$$

This equation, in combination with (2.36), gives a relationship between V_G and T_G; the differential equation satisfied by $T_G(r, z)$ may be obtained by using (2.14) to eliminate u in (2.16) and then eliminating V_G using (2.36). The result is

$$\nabla^2\theta - \frac{2}{r}\frac{\partial}{\partial r}\left\{\frac{\sigma - 1}{\sigma}\theta\right\} = -2hr\left\{\nabla^2 - \frac{1}{r^2}\right\}P(r) + \epsilon_f E^{-\frac{1}{2}}\rho_e(r)\left\{\frac{Pr - 1 + \sigma}{\sigma}\right\}W_G\frac{\partial\theta}{\partial z}, \tag{2.40}$$

where

$$\theta = \sigma T_G. \tag{2.41}$$

Note that for $\epsilon_f \ll E^{\frac{1}{2}}$ the last term in (2.40) is negligible, but for $\epsilon_f = O(E^{\frac{1}{2}})$ it is comparable to the other terms; a similar convection effect appears in the study of Homsy & Hudson (1969). On the other hand, for $E^{\frac{1}{2}} \ll \epsilon_f \ll E^{\frac{1}{4}}$, the solution for θ has a boundary-layer character (for $W_G \neq 0$). It will be demonstrated that in this case thermal layers of width $O(E^{\frac{1}{4}}/\epsilon_f^{\frac{1}{2}})$ occur on $r = a$ and b; in addition, on either $z = 0$ or $z = 1$ a layer of width $O(E^{\frac{1}{2}}/\epsilon_f)$ is present. Note that these layers are thicker than the velocity boundary layers on the corresponding wall. The boundary conditions for this equation will be discussed in §§ 2.3–2.5.

The geostrophic flow due to three separate effects will now be considered in §§2.3–2.5; these effects are the source–sink flow, denoted by subscript S (§2.3); a mechanical differential rotation of the end plates, denoted by subscript M (§2.4); and an applied thermal gradient, denoted by subscript T (§2.5). In the flow regime $\epsilon_f \ll E^{\frac{1}{4}}$, the results of any combination of the three solutions due to each effect may be superimposed.

2.3. *Source–sink flow*

In the present centrifuge configuration, it is assumed that the injection and withdrawal occurs either in the corner regions of the container or at one or more locations along the vertical sidewalls. The net mass-flow rate entering the container from the inner radius is given by (2.6), and, since $u = O(E)$ in the core, the incoming mass-flow rate must be balanced by the radial flow in the Ekman layers given by (2.34); consequently it follows that

$$V_{GS}(r, 1) + V_{GS}(r, 0) = -\frac{2a}{r\sigma^{\frac{1}{4}}\rho_e^{\frac{1}{2}}}, \tag{2.42}$$

where the subscript S is used to denote that part of the complete solution due to the source–sink flow. Substitution in (2.39) (with $T_B = V_B = 0$ at $z = 0, 1$) yields

$$P_S(r) = -\frac{a\sigma^{\frac{3}{4}}}{r\rho_e^{\frac{1}{2}}}, \tag{2.43}$$

and it follows from (2.32) and (2.39) that the geostrophic azimuthal velocity and temperature distributions near the upper and lower end plates are given by

$$V_{GS}(r,0) = V_{GS}(r, 1) = \frac{P_S(r)}{\sigma(r)}, \tag{2.44}$$

$$T_{GS}(r,0) = T_{GS}(r, 1) = \frac{-2hr\,P_S(r)}{\sigma(r)}. \tag{2.45}$$

Furthermore, it then follows from the Ekman conditions (2.35) and the last of (2.27) that

$$W_{GS}(r) = 0, \tag{2.46}$$

and thus the source–sink flow induces no vertical motion in the core, to leading order.

To complete specification of the boundary conditions for V_{GS} and T_{GS}, the vertical shear layers at $r = a$ and $r = b$ must be considered, and using a procedure similar to that leading to (2.31), it may be shown (see §2.6) that to leading order $T + 2hrv$ is constant in the radial direction across the sidewall boundary layers; thus

$$T_{GS}(r_0, z) + 2hr_0\,V_{GS}(r_0, z) = 0, \tag{2.47}$$

where $r_0 = a$ or b. Using (2.36) and (2.47), it follows that the geostrophic azimuthal velocity and temperature distributions near the sidewalls are given by

$$V_{GS}(r_0, z) = \frac{P_S(r_0)}{\sigma(r_0)}, \quad T_{GS}(r_0, z) = \frac{-2hr_0\,P_S(r_0)}{\sigma(r_0)}. \tag{2.48}$$

For $\epsilon_f \ll E^{\frac{1}{4}}$, the interior geostrophic solution may be obtained by solving equation (2.40) either numerically by standard relaxation techniques (Bark & Hultgren 1979) or by expanding in a power series for small h; details are omitted for brevity.

2.4. *Differential rotation*

In a mechanically driven centrifuge, one or both end plates are rotated at a slightly different rate from the vertical sidewalls, and this has the effect of inducing a vertical

drift velocity in the geostrophic core region. The solution for this effect will be denoted by a subscript M and has homogeneous boundary conditions for the temperature on all walls and boundary conditions for v given by (2.26). Across any radial surface there can exist no net mass flux associated with the differential rotation and consequently the radial flows in the Ekman layers on the upper and lower plates must exactly balance; using (2.26) and (2.34) it follows that

$$V_{\mathrm{GM}}(r,1)+V_{\mathrm{GM}}(r,0)=V_{\mathrm{B}}(r,0)+V_{\mathrm{B}}(r,1)=(\lambda_0+\lambda_1)\lambda_{\mathrm{m}}r. \tag{2.49}$$

Substitution in (2.39) yields

$$P_{\mathrm{M}}(r)=\tfrac{1}{2}(\lambda_0+\lambda_1)\lambda_{\mathrm{m}}r, \tag{2.50}$$

and it follows from (2.32), (2.36) and (2.50) that the geostrophic azimuthal velocity and temperature distributions near the upper and lower plate are given by

$$V_{\mathrm{GM}}(r,0)=\frac{r\lambda_{\mathrm{m}}}{2\sigma}(\lambda_0+\lambda_1+2h\lambda_0 r^2),\quad V_{\mathrm{GM}}(r,1)=\frac{r\lambda_{\mathrm{m}}}{2\sigma}(\lambda_0+\lambda_1+2h\lambda_1 r^2), \tag{2.51}$$

$$T_{\mathrm{GM}}(r,0)=-\frac{\lambda_{\mathrm{m}}hr^2}{\sigma}(\lambda_1-\lambda_0),\quad T_{\mathrm{GM}}(r,1)=\frac{\lambda_{\mathrm{m}}hr^2}{\sigma}(\lambda_1-\lambda_0). \tag{2.52}$$

The boundary conditions near the sidewalls are obtained by using (2.46) and a relation analogous to (2.50), and these are

$$V_{\mathrm{GM}}=\frac{\lambda_{\mathrm{m}}r_0}{2\sigma(r_0)}(\lambda_0+\lambda_1),\quad T_{\mathrm{GM}}=-\frac{\lambda_{\mathrm{m}}hr_0^2}{\sigma(r_0)}(\lambda_1+\lambda_0), \tag{2.53}$$

where $r_0=a$ or b. The vertical velocity in the core is obtained by using the Ekman conditions (2.35) and the equations (2.51), and is given by

$$W_{\mathrm{GM}}(r)=\frac{\lambda_{\mathrm{m}}(\lambda_1-\lambda_0)}{4r\rho_{\mathrm{e}}(r)}\frac{\partial}{\partial r}\left\{\frac{r^2\rho_{\mathrm{e}}^{\frac{1}{2}}}{\sigma^{\frac{3}{4}}}\right\}. \tag{2.54}$$

For $\epsilon_{\mathrm{f}}=O(E^{\frac{1}{2}})$, (2.40) may be solved, subject to the conditions (2.52) and (2.53), for the differential rotation component of the temperature field. This may be done numerically or as a perturbation expansion for small h; the details are omitted.

In the parameter range $E^{\frac{1}{2}}\ll\epsilon_{\mathrm{f}}\ll E^{\frac{1}{4}}$, the thermal problem becomes a singular perturbation problem. Defining $s=\mathrm{sgn}\{W_{\mathrm{G}}(r)\}$, the interior solution is given by

$$\theta=\theta_{\mathrm{M}}=h\lambda_{\mathrm{m}}(\lambda_1-\lambda_0)sr^2. \tag{2.55}$$

This solution satisfies the boundary conditions at $z=\frac{1}{2}(1-s)$, but a thermal boundary layer having a thickness $O(E^{\frac{1}{2}}/\epsilon_{\mathrm{f}})$ is required at $z=\frac{1}{2}(1+s)$. Define a scaled boundary-layer variable ζ' according to

$$\zeta'=\frac{s\rho_{\mathrm{e}}(r)\,W_{\mathrm{G}}(r)}{\sigma(r)\,E^{\frac{1}{2}}}\{Pr-1+\sigma(r)\}\,\epsilon_{\mathrm{f}}\{z-\tfrac{1}{2}(1+s)\}. \tag{2.56}$$

The boundary-layer solutions at $z=\frac{1}{2}(1+s)$ are

$$\theta_{\mathrm{M}}=h\lambda_{\mathrm{m}}(\lambda_1-\lambda_0)sr^2(1-2e^{-\zeta'}). \tag{2.57}$$

At $r=a$ and b, sidewall boundary layers are required to adjust the core solution (2.55) to the correct values on the sidewalls. Define a scaled radial coordinate ξ' according to

$$\xi'=\beta(r-r_0)\left[\frac{s\epsilon_{\mathrm{f}}}{\sigma(r_0)}\rho_{\mathrm{e}}(r_0)\,W_{\mathrm{G}}(r_0)\{Pr-1+\sigma(r_0)\}\right]^{\frac{1}{2}}E^{-\frac{1}{4}}, \tag{2.58}$$

where $\beta = 1$ at $r_0 = a$ and $\beta = -1$ at $r_0 = b$; the sidewall thermal layers originate at $z = \frac{1}{2}(1-s)$ and the boundary-layer solution is given by

$$\theta_M = h\lambda_m(\lambda_1 - \lambda_0)\, s r_0^2 \operatorname{erf} z' - h\lambda_m(\lambda_1 + \lambda_0)\, r_0^2 \operatorname{erfc} z', \tag{2.59}$$

where $z' = \frac{1}{2}\xi'/\{s(z-\frac{1}{2}(1-s)\}$. Note that the sidewall thermal layers and the thermal layer on the end wall have thicknesses $O(E^{\frac{1}{4}}/\epsilon_f^{\frac{1}{2}})$ and $O(E^{\frac{1}{2}}/\epsilon_f)$ respectively, and consequently are much thicker than any velocity boundary layers, which have a maximum thickness $O(E^{\frac{1}{4}})$.

2.5. *Applied thermal gradient*

In a thermally driven centrifuge, a vertical drift velocity is induced in the geostrophic core region by imposing a thermal gradient between the horizontal endplates. For this problem, the velocity boundary conditions are homogeneous at all solid walls, and the temperature boundary condtions are given by (2.22) and (2.23). As in §2.4, no net mass flux due to the thermally induced motion can exist across any cylindrical control surface, and thus the radial flows in the Ekman layers must be equal, and opposite in direction. Using a subscript T to denote the thermally induced motion, it follows from (2.34) that

$$V_{GT}(r, 1) + V_{GT}(r, 0) = 0, \tag{2.60}$$

and substitution in (2.39), using (2.22), gives

$$P_T(r) = -\tfrac{1}{4}\lambda_T r. \tag{2.61}$$

It follows from (2.32), (2.36) and (2.61) that the geostrophic azimuthal velocity and temperature distributions near the upper and lower plates are given by

$$V_{GT}(r, 1) = -V_{GT}(r, 0) = \frac{r\lambda_T}{4\sigma}, \tag{2.62}$$

$$T_{GT}(r, 0) = \lambda_T - T_{GT}(r, 1) = \frac{hr^2\lambda_T}{2\sigma}. \tag{2.63}$$

The boundary values near the sidewalls of the azimuthal velocity and temperature follow from (2.23), (2.36) and the fact that $T + 2hrv$ is invariant in the radial direction across the vertical shear layers; these conditions are

$$V_{GT}(a, z) = \frac{a\lambda_T}{2\sigma(a)}\{\lambda_a - \tfrac{1}{2}\}, \quad T_{GT}(a, z) = \frac{\lambda_T}{\sigma(a)}\{\lambda_a + \tfrac{1}{2}ha^2\} \tag{2.64}$$

at $r = a$, with similar conditions at $r = b$, which may be obtained by replacing a by b in (2.64). The vertical velocity in the core may be obtained from the Ekman conditions (2.35) and the equations (2.62), and it follows that

$$W_{GT}(r) = -\frac{\lambda_T}{8r\rho_e(r)}\frac{\partial}{\partial r}\left\{\frac{r^2\rho_e^{\frac{1}{2}}}{\sigma^{\frac{3}{4}}}\right\}. \tag{2.65}$$

Consequently, the applied thermal gradient induces a downward vertical drift $O(E^{\frac{1}{2}})$ from the upper to the lower Ekman layer; it is of interest to note that this drift velocity only differs by a constant from that given for a mechanically driven centrifuge in (2.54).

For $\epsilon_f = O(E^{\frac{1}{2}})$, (2.40) may be solved numerically to determine the interior temperature distribution, while for $E^{\frac{1}{2}} \ll \epsilon_f \ll E^{\frac{1}{4}}$ a singular perturbation solution similar to that described in §2.4 may readily be obtained.

2.6. *The $E^{\frac{1}{4}}$ layers*

An $E^{\frac{1}{4}}$ layer is necessary to reduce the azimuthal velocity to relative rest on each of the container sidewalls; define a boundary-layer variable ξ and a constant α according to

$$\xi = \beta(r-r_0)\,\alpha E^{-\frac{1}{4}}, \quad \alpha = \sqrt{2}\,\sigma^{\frac{1}{8}}(r_0)\,\rho_e^{\frac{1}{2}}(r_0), \tag{2.66}$$

where $\beta = 1$ at $r_0 = a$ and $\beta = -1$ for $r_0 = b$. The solutions for the leading terms in the $E^{\frac{1}{4}}$ layer solution may be computed with standard techniques (Walker & Stewartson 1972; Matsuda & Hashimoto 1978) and are given by

$$v_{\frac{1}{4}} = V_G(r_0)\,(1-e^{-\xi}) + \ldots, \quad T_{\frac{1}{4}} = T_B(r_0,z) - 2hr_0\,V_G(r_0)\,(1-e^{-\xi}) + \ldots, \tag{2.67a, b}$$

$$w_{\frac{1}{4}} = -\frac{\beta\alpha\sigma^{\frac{1}{4}}(r_0)}{\rho_e^{\frac{1}{2}}(r_0)}\,V_G(r_0)\,E^{\frac{1}{4}}(z-\tfrac{1}{2})\,e^{-\xi} + \ldots, \quad u_{\frac{1}{4}} = -\frac{\alpha^2 V_G(r_0)}{2\rho_e(r_0)}\,E^{\frac{1}{2}}e^{-\xi} + \ldots. \tag{2.67c, d}$$

Here $V_G(r_0)$ is the limiting form of $V_G(r, z)$ for either of the three effects given by (2.48), (2.53) or (2.64), as $r \to r_0$ (where $r_0 = a$ or b).

2.7. *The $E^{\frac{1}{4}} \times E^{\frac{1}{4}}$ regions*

In the Ekman-layer extensions, which are above and below the $E^{\frac{1}{4}}$ layers, $\partial/\partial r \sim E^{-\frac{1}{4}}$ and $\partial/\partial z \sim E^{-\frac{1}{2}}$, and it may readily be deduced that in these regions

$$\frac{\partial^2}{\partial z^2}(T + 2hr_0\,v) = 0, \tag{2.68}$$

or that

$$T + 2hr_0\,v = T_B(r_0+,\,z_0) + 2hr_0\,V_B(r_0+,\,z_0), \tag{2.69}$$

where $z_0 = 0$ or 1.† Using (2.67*a*, *b*), it can be shown that unless there is no differential rotation ($V_B(r_0+,\,z_0) = 0$) and, in addition, unless the endwalls and sidewalls are at the same temperature ($T_B(r_0+,\,z_0) = T_B(r_0,\,z_0)$), then the $E^{\frac{1}{4}}$ layer solution is not compatible with the solution in the vertical direction. In this region, the velocity components, pressure and temperature are written, to leading order, as

$$v = \tilde{v}(\xi,\,\zeta^*) + \ldots, \quad T = \tilde{T}(\xi,\,\zeta^*) + \ldots, \tag{2.70a, b}$$

$$u = \frac{\alpha^2}{2\rho_e(r_0)}\,E^{\frac{1}{4}}\tilde{u}(\xi,\,\zeta^*) + \ldots, \quad w = \frac{\beta\alpha\sigma^{\frac{1}{4}}(r_0)}{\rho_e^{\frac{1}{2}}(r_0)}\,E^{\frac{1}{4}}\tilde{w}(\xi,\,\zeta^*) + \ldots, \tag{2.70c, d}$$

$$p = \frac{\beta M^2}{\alpha}\,E^{\frac{1}{4}}\tilde{p}(\xi,\,\zeta^*). \tag{2.70e}$$

Here ξ and β are the scaled variable and constant associated with the $E^{\frac{1}{4}}$ layer and defined in (2.66). In addition, ζ^* is the scaled vertical variable defined by $\zeta^* = \alpha(1-z)\,E^{-\frac{1}{4}}$ or $\zeta^* = \alpha z E^{-\frac{1}{4}}$ near $z = 1$ and 0 respectively; α is the constant defined in (2.66). The necessity of these $E^{\frac{1}{4}} \times E^{\frac{1}{4}}$ regions in steady rotating flows was apparently first recognized by Matsuda & Hashimoto (1978), who considered the case of insulated endplates and conducting sidewalls; however, the authors did not give a solution for the corner regions. The steady problem is also discussed heuristically by Bark & Hultgren (1979); similar problems are mentioned in Hultgren, Meijer & Bark (1981) and Bark, Meijer & Cohen (1978) for unsteady rotating flows, but solutions were not obtained.

Substitution in (2.12)–(2.16) leads to the following equations:

$$-2\tilde{v} + r_0\,\tilde{T} + \frac{\partial\tilde{p}}{\partial\xi} = 0, \tag{2.71}$$

† r_0+ denotes either $a+$ or $b-$.

$$\tilde{u} = \nabla_1^2 \tilde{v}, \tag{2.72}$$

$$-2hr_0 \tilde{u} = \nabla_1^2 \tilde{T}, \tag{2.73}$$

$$\frac{\partial \tilde{p}}{\partial \zeta^*} = \frac{\partial \tilde{w}}{\partial \zeta^*} = 0, \tag{2.74}$$

where

$$\nabla_1^2 = \frac{\partial^2}{\partial \xi^2} + \frac{\partial^2}{\partial \zeta^{*2}}.$$

It follows from the second of (2.74) that

$$\tilde{w} = -V_G(r_0)(z_0 - \tfrac{1}{2}) e^{-\xi}, \tag{2.75}$$

in order to match the $E^{\frac{1}{4}}$ layer solution, where $z_0 = 0$ or 1. Thus since u is $O(E^{\frac{1}{2}})$ and of lower order, the streamlines in a cross-section pass vertically straight through this region. According to the first of (2.74), the pressure in (2.71) may be eliminated by differentiation to obtain

$$2\frac{\partial \tilde{v}}{\partial \zeta^*} = r_0 \frac{\partial \tilde{T}}{\partial \zeta^*},$$

and consequently

$$\tilde{T} = \frac{2}{r_0}\tilde{v} + H(\xi), \tag{2.76}$$

where the arbitrary function $H(\xi)$ is determined by matching to the $E^{\frac{1}{4}}$ layer in the limit $\zeta^* \to \infty$. This gives†

$$H(\xi) = T' - \frac{2}{r_0} V = T_B(r_0, z) - \frac{2\sigma(r_0)}{r_0} V_G(r_0)(1 - e^{-\xi}). \tag{2.77}$$

Equation (2.77) with (2.76) gives one relation between $\tilde{v}$ and $\tilde{T}$, and, to obtain a second relation, (2.72) and (2.73) are combined to give

$$\nabla_1^2 \phi = 0, \tag{2.78}$$

where

$$\phi = \tilde{T} + 2hr_0 \tilde{v}. \tag{2.79}$$

The solution of (2.78) is now required, subject to the conditions

$$\phi = \phi_0 = T_B(r, z_0) + 2hr_0 V_B(r, z_0) \quad \text{on} \quad \zeta^* = 0,$$

to match the Ekman extensions; here $z_0 = 0$, 1. In addition

$$\phi = \phi_1 = T_B(r_0, z) \quad \text{as} \quad \xi \to 0, \tag{2.80}$$

where $r_0 = a$ or b. The solution is

$$\phi = \phi_0 + \frac{2}{\pi}(\phi_1 - \phi_0) \arctan \frac{\zeta^*}{\xi}, \tag{2.81}$$

and combining with (2.76) yields

$$\tilde{v} = V(\xi, z_0) + \frac{r_0(\phi_1 - \phi_0)}{2\sigma(r_0)}\left\{-1 + \frac{2}{\pi}\arctan\frac{\zeta^*}{\xi}\right\}, \tag{2.82}$$

$$\tilde{T} = T'(\xi, z_0) + \frac{\phi_1 - \phi_0}{\sigma(r_0)}\left\{-1 + \frac{2}{\pi}\arctan\frac{\zeta^*}{\xi}\right\}, \tag{2.83}$$

$$\tilde{u} = U(\xi, z_0). \tag{2.84}$$

Note that the $E^{\frac{1}{4}} \times E^{\frac{1}{4}}$ regions are passive in nature and are a direct consequence of an irregularity in the geostrophic solution in any situation where differential rotation

† T' is the temperature in the $E^{\frac{1}{4}}$ layer.

occurs or where a difference in temperature exists between the endwall and sidewall. In this region an adjustment between the $E^{\frac{1}{4}}$ layer and Ekman extension occurs vertically.

2.8. *The $E^{\frac{1}{3}}$ layers*

As $\xi \to 0$ for fixed z, the radial velocity in the $E^{\frac{1}{4}}$ layer does not in general approach the correct boundary conditions at the wall and an $E^{\frac{1}{3}}$ layer is required for this adjustment. The form of the $E^{\frac{1}{3}}$ layer expansions is determined by expanding the $E^{\frac{1}{4}}$ layer solutions given by (2.67) in a Taylor series for small ξ and by rewriting these expansions in terms of the $E^{\frac{1}{3}}$ layer variable η defined by

$$\eta = \rho_{\mathrm{e}}^{\frac{1}{3}}(r_0)\,\sigma^{\frac{1}{6}}(r_0)\,\beta(r-r_0)\,E^{-\frac{1}{3}} \tag{2.85}$$

where $r_0 = a$ or b, and β is defined in connection with (2.66). The velocity expansions in the $E^{\frac{1}{3}}$ layer are of the form

$$v_{\frac{1}{3}} = \frac{\sqrt{2}\,\eta\,V_{\mathrm{G}}(r_0)}{\rho_{\mathrm{e}}^{\frac{1}{12}}\sigma^{\frac{1}{24}}}E^{\frac{1}{12}} - \frac{V_{\mathrm{G}}(r_0)\,E^{\frac{1}{6}}}{\rho_{\mathrm{e}}^{\frac{1}{6}}\sigma^{\frac{1}{12}}}v_2(\eta, z) + \ldots, \tag{2.86}$$

$$w_{\frac{1}{3}} = -\frac{\beta\,V_{\mathrm{G}}(r_0)\,\sigma^{\frac{5}{12}}}{\rho_{\mathrm{e}}^{\frac{1}{6}}}E^{\frac{1}{6}}w_2(\eta, z) + \ldots, \tag{2.87}$$

$$u_{\frac{1}{3}} = -\frac{V_{\mathrm{G}}(r_0)\,\sigma^{\frac{1}{4}}}{\rho_{\mathrm{e}}^{\frac{1}{2}}}E^{\frac{1}{2}}u_2(\eta, z) + \ldots. \tag{2.88}$$

Here the functions ρ_{e} and σ are evaluated at $r = r_0$. The temperature and azimuthal velocity are related to each other by

$$T_{\frac{1}{3}}(\eta, z) + 2hr_0\,v_{\frac{1}{3}}(\eta, z) = T_{\mathrm{B}}(r_0, z), \tag{2.89}$$

which follows upon combination of the leading-order form of (2.14) and (2.16) in the $E^{\frac{1}{3}}$ layer. Note that the first term in (2.86) is $O(E^{\frac{1}{12}})$ and is a regular solution corresponding to the continuation of the $E^{\frac{1}{4}}$ layer solution into the $E^{\frac{1}{3}}$ layer. The other terms in (2.86)–(2.88) describe the structure of the $E^{\frac{1}{3}}$ layer, and in general are not regular (Conlisk & Walker 1981); in the case of injection or withdrawal at the sidewall through slots having a width $O(E^{\frac{1}{2}})$, the $E^{\frac{1}{3}}$ layer sees such locations as point sources or sinks respectively, and the solution for (u_2, v_2, w_2) will be singular there. In the case of differential rotation the $E^{\frac{1}{3}}$ layer solution is irregular near the corners of the container. In any case, the equations satisfied by the terms in (2.86)–(2.88) are

$$\frac{\partial^3 v_2}{\partial \eta^3} = -2\frac{\partial w_2}{\partial z}, \quad \frac{\partial^3 w_2}{\partial \eta^3} = 2\frac{\partial v_2}{\partial z}, \quad \frac{\partial u_2}{\partial \eta} + \frac{\partial w_2}{\partial z} = 0, \tag{2.90}$$

which may be obtained from (2.12)–(2.15). The boundary conditions are the matching conditions to the $E^{\frac{1}{4}}$ layer, given by

$$v_2 \sim \eta^2, \quad w_2 \to 0, \quad u_2 \to 1 \quad \text{as} \quad \eta \to \infty, \tag{2.91}$$

and the conditions on the sidewalls, that

$$u_2 = w_2 = v_2 = 0 \quad \text{at} \quad \eta = 0, \tag{2.92}$$

except at points of injection or withdrawal. Furthermore, the Ekman conditions in (2.35) require that

$$w_2 = 0 \quad \text{at} \quad z = 0, 1 \quad \text{for} \quad \eta > 0. \tag{2.93}$$

Solutions of (2.90) subject to the conditions (2.91)–(2.93) have recently been considered by Conlisk & Walker (1981) in connection with incompressible source–sink

flow; these solutions are of two types. Consider first the case where injection occurs through axisymmetric slots having a width $O(E^{\frac{1}{2}})$ in the corners on the inner wall of the container; in view of the Ekman condition (2.93) the fluid cannot enter the $E^{\frac{1}{3}}$ layer via the Ekman extension above or below the $E^{\frac{1}{3}}$ layer. Consequently a region having vertical and horizontal dimensions $O(E^{\frac{1}{2}})$ will exist about the point of injection; on the scale of the $E^{\frac{1}{3}}$ layer this region appears as a point source and the $E^{\frac{1}{3}}$ layer solution must become singular as such a region is approached. Conlisk & Walker (1981) have obtained the solution for such injection in an integral form that contains the singular behaviour explicitly; the solution may also be written as a Fourier series at locations away from the corners, and the result is

$$w_2(\eta, z) = \frac{8}{\sqrt{3}} \sum_{n=1}^{\infty} \left\{ \frac{C + C'(-1)^n}{\omega_n^2} \right\} e^{-\omega_n \eta/2} \sin(\tfrac{1}{2}\sqrt{3}\, \omega_n \eta) \sin n\pi z, \tag{2.94}$$

where $\omega_n = (2n\pi)^{\frac{1}{3}}$. The solution (2.94) describes the $E^{\frac{1}{3}}$ layer flow due to sources of relative strengths C and C' at $r = a$, $z = 0$ and 1 respectively, such that

$$C + C' = 1, \tag{2.95}$$

and the volumetric flux per unit length of circumference associated with this solution in the $E^{\frac{1}{3}}$ layer is

$$\int_0^{\infty} w_2(\eta, z)\, d\eta = C(1-z) - C'z, \tag{2.96}$$

at any height z. The corresponding solution for the radial velocity is

$$u_2 = 1 + \frac{4}{\sqrt{3}} \sum_{n=1}^{\infty} \{C + (-1)^n C'\} e^{-\omega_n \eta/2} \sin(\tfrac{1}{2}\sqrt{3}\, \omega_n \eta + \tfrac{1}{3}\pi) \cos n\pi z$$
$$- 2C \sum_{n=-\infty}^{\infty} \delta(z - 2n) - 2C' \sum_{n=-\infty}^{\infty} \delta(z - 2n - 1). \tag{2.97}$$

Here $\delta(z)$ is the Dirac delta-function. The solution given by (2.94) and (2.97) also describe the flow in the $E^{\frac{1}{3}}$ layer on the outer wall at $r = b$ due to sinks of relative strength C and C' at $z = 0$ and 1 respectively.

The second type of $E^{\frac{1}{3}}$ layer solution of interest corresponds to injection or withdrawal through an axisymmetric slot having a vertical dimension $O(E^{\frac{1}{2}})$. A square region having dimensions $O(E^{\frac{1}{2}})$ will exist near the slot, and on the scale of the $E^{\frac{1}{3}}$ layer this region appears as a point source or sink. Conlisk & Walker (1981) give the solution for a point source on the inner wall, or alternatively for a sink on the outer wall, at $z = \phi$; the Fourier-series representation is

$$w_2 = \frac{8}{\sqrt{3}} \sum_{n=1}^{\infty} \frac{\cos n\pi\phi}{\omega_n^2} e^{-\omega_n \eta/2} \sin(\tfrac{1}{2}\sqrt{3}\, \omega_n \eta) \sin n\pi z, \tag{2.98}$$

$$u_2 = 1 + \frac{4}{\sqrt{3}} \sum_{n=1}^{\infty} \cos n\pi\phi\, e^{-\omega_n \eta/2} \sin\{\tfrac{1}{2}\sqrt{3}\, \omega_n \eta + \tfrac{1}{3}\pi\} \cos n\pi z \tag{2.99}$$
$$- \sum_{\substack{n=-\infty \\ n \neq 0}}^{\infty} \delta(z - \phi - 2n) - \sum_{n=-\infty}^{\infty} \delta(z + \phi - 2n).$$

The vertical flux associated with this solution in the $E^{\frac{1}{3}}$ layer is

$$\int_0^{\infty} w_2(\eta, z)\, d\eta = 1 - z \quad \text{for} \quad z > \phi, \tag{2.100a}$$
$$= -z \quad \text{for} \quad z < \phi. \tag{2.100b}$$

The only other possible type of axisymmetric injection or withdrawal on the sidewalls is the distributed source having a vertical dimension $O(1)$; the solution in this case is also given by Conlisk & Walker (1981), but the results are not included here.

It remains to consider the $E^{\frac{1}{3}}$ layer flow due to differential rotation and the applied thermal gradient; in the former case the $E^{\frac{1}{3}}$ layer solution for (u_2, v_2, w_2) is irregular in the corner region when the endplate is in differential rotation. Outside the Ekman extension adjacent to the $E^{\frac{1}{3}}$ layer, the azimuthal and radial velocities are given by (2.86) and (2.88) and the leading terms are $O(E^{\frac{1}{12}})$ and $O(E^{\frac{1}{2}})$ respectively; however, the leading-order terms for u and v are $O(1)$ in the Ekman extension and therefore arise purely from the differential rotation. It follows from (2.35) that there is a radial mass flux outward in each Ekman extension equal to $\frac{1}{2}\rho_e^{\frac{1}{2}}(r_0)\,\sigma^{\frac{1}{4}}(r_0)\,V_B(r_0+, z)\,E^{\frac{1}{2}}$; this flux must be balanced by a vertical flux $O(E^{\frac{1}{2}})$ in the $E^{\frac{1}{3}}$ layer. However, in view of the Ekman compatibility condition in (2.93), the flux cannot enter or leave the Ekman extension for $\eta > 0$. In fact, the fluid enters or leaves the $E^{\frac{1}{3}}$ layer via an $E^{\frac{1}{2}} \times E^{\frac{1}{2}}$ region in the corner of the container and on the scale of the $E^{\frac{1}{3}}$ layer this region appears as either a point source or point sink. To balance the influx in the Ekman extension it follows from (2.87) that

$$\int_0^\infty w_2(\eta, z_0)\,d\eta = -\frac{V_B(r_0+, z_0)}{2\,V_{GM}(r_0)}. \tag{2.101}$$

The solution given by (2.94) is due to point sources at the inner wall of strengths C and C' at $z = 0$ and 1 respectively. The $E^{\frac{1}{3}}$ layer solution for differential rotation may be obtained from (2.53) and (2.101) by using

$$C = -\frac{\lambda_0\,\sigma(r_0)}{2(\lambda_0+\lambda_1)}, \quad C' = -\frac{\lambda_1\,\sigma(r_0)}{2(\lambda_0+\lambda_1)} \tag{2.102}$$

in (2.94). Note that (2.102) do not apply for the antisymmetric case $\lambda_0+\lambda_1 = 0$; in this case there is no azimuthal geostrophic motion (see (2.53)) at the sidewalls and consequently no $E^{\frac{1}{4}}$ layers; for this situation, the expansions in (2.86)–(2.88) for the $E^{\frac{1}{3}}$ layer must be modified.

The $E^{\frac{1}{3}}$ layer solutions for the thermally induced motion are also irregular in any corner of the container where the sidewall temperature is not equal to the temperature of the end wall; in such cases the solution is also given by (2.94), but with

$$C = \frac{\lambda_a}{2\lambda_a - 1}, \quad C' = \frac{\lambda_a - 1}{2\lambda_a - 1}, \tag{2.103}$$

on $r = a$. The corresponding solution on $r = b$ is obtained by replacing a by b in (2.103).

Finally, it is of interest to note that an $E^{\frac{1}{3}} \times E^{\frac{1}{3}}$ region similar to the $E^{\frac{1}{4}} \times E^{\frac{1}{4}}$ region described in §2.7 will exist between the $E^{\frac{1}{3}}$ layer and the Ekman extensions if either differential rotation occurs or if the sidewall and endwall are maintained at different temperatures. These square regions are passive in nature and exist to provide an adjustment in the vertical direction between the $E^{\frac{1}{3}}$ layer and the Ekman extension. The solutions in this region are similar to those described in §2.7.

2.9. *Summary*

In the present study, solutions have been obtained for the velocity components and temperature distribution in a model centrifuge consisting of a pair of concentric cylinders bounded by horizontal end plates in a state of rapid rotation about the axis of the cylinders. It has been assumed that there is a net source–sink flow of a binary

gas from the inner to the outer radius, and further that the walls are maintained at a constant temperature. The source–sink flow induces no radial or vertical motion within the geostrophic core; two effects that induce a vertical velocity $O(E^{\frac{1}{2}})$ have been considered: namely a thermal gradient applied vertically and differential rotation of one or both the endplates. Note that in §§2.3–2.5 a boundary-value problem for V_G and T_G has been formulated for the source–sink, thermal-gradient and differential-rotation problems respectively; these interior problems have not been solved explicitly for the case $\epsilon_f = O(E^{\frac{1}{2}})$, but the values of V_G and T_G are determined around the perimeter of the geostrophic core. For small h, the geostrophic problems may be approached as a regular perturbation problem as previously indicated; for $h = O(1)$ the geostrophic problem may be calculated by standard numerical methods (see e.g. Bark & Hultgren 1979). This aspect has not been pursued in detail here since, for the mass-transfer problem considered in §3, the self-diffusion coefficient of the binary gas mixture is independent of temperature to leading order. Consequently the core temperature distribution is not of primary importance in the parameter range considered.

It is worthwhile to note that it has been assumed that the rotational Mach number M is $O(1)$, and thus the present theory does not hold for high-speed centrifuges ($M^2 \gg 1$). More specifically, it has been assumed that the density does not vary across the shear layers. The thickest shear layer is the $E^{\frac{1}{4}}$ layer; it may be shown, upon expanding (2.5) in a Taylor series about $r = a$ or b and using (2.66), that the present analysis applies to the parameter range $M^2 E^{\frac{1}{4}} \ll 1$. Note that this is within the practical ranges for M^2 and E for centrifuges quoted by Soubbaramayer (1979).

One important feature that enters the boundary conditions in the mass-transfer problem is the volumetric flux in the boundary layers. In the model centrifuge these fluxes are $O(E^{\frac{1}{2}})$; define a dimensionless volumetric flux $\mathscr{F}_\alpha$ per unit length of circumference in terms of the actual volumetric flux $\mathscr{F}_\alpha^*$ by

$$\mathscr{F}_\alpha^* = \frac{\dot{m}_0^* E^{\frac{1}{2}}}{\rho_0^* L} \mathscr{F}_\alpha, \tag{2.104}$$

where $\dot{m}_0^*$ is defined in (2.6) and α is a subscript associated with the boundary layer in question. For each Ekman layer it follows from (2.34) that there is a net volumetric flux radially outward per unit length of circumference given by

$$\mathscr{F}_{\frac{1}{2}}(r, z_0) = \frac{\sigma^{\frac{1}{4}}}{2\rho_e^{\frac{1}{2}}} \{V_B(r, z_0) - V_G(r, z_0)\}, \tag{2.105}$$

where $z_0 = 0$ or 1, and V_G is given by either (2.44), (2.51) or (2.62), or the sum of two or more of these equations.

The volumetric flux per unit length of circumference in the positive z-direction for the sidewall boundary layer is denoted by $\mathscr{F}_s$ and consists of the sum of the $E^{\frac{1}{4}}$ and $E^{\frac{1}{3}}$ layer fluxes given by

$$\mathscr{F}_{\frac{1}{4}}(r_0) = -\frac{\beta\sigma^{\frac{1}{4}}(r_0)}{\rho_e^{\frac{1}{2}}(r_0)} V_G(r_0)\,(z - \tfrac{1}{2}), \tag{2.106}$$

$$\mathscr{F}_{\frac{1}{3}}(r_0) = -\frac{\beta\sigma^{\frac{1}{4}}(r_0)}{\rho_e^{\frac{1}{2}}(r_0)} V_G(r_0) \int_0^\infty w_2(\eta, z)\, d\eta. \tag{2.107}$$

Here $r_0 = a$ or b, and V_G is given by either of (2.48), (2.53) or (2.64) or by the sum of two or more of these effects. The integral in (2.107) depends upon the placement of the sources and sinks on the sidewalls, and two possibilities are given in (2.96) and (2.100).

It is now possible to consider the problem of how the binary gas can undergo a separation process within the model centrifuge, and this question is addressed in §3.

3. Mass transfer

3.1. *Formulation*

The mass-transfer equation for the centrifuge expresses the fact that the total mass of species A within the gas mixture is conserved. The absolute mass flux of species A is denoted by $\mathbf{n}_A^*$ and is defined by

$$\mathbf{n}_A^* = \rho_A^* \mathbf{q}_A^*, \tag{3.1}$$

where $\mathbf{q}_A^*$ is the absolute velocity of species A, and ρ_A^* is the mass of species A per unit volume of solution. The flux of species A relative to the mass average velocity $\mathbf{q}^*$ (calculated in §2) is denoted by $\mathbf{j}_A^* = \rho_A^*(\mathbf{q}_A^* - \mathbf{q}^*)$. Using (3.1), it is apparent that

$$\mathbf{n}_A^* = \mathbf{j}_A^* + \rho_A^* \mathbf{q}^*. \tag{3.2}$$

In the species-separation problems associated with gas centrifuges, the two primary effects contributing to $\mathbf{j}_A^*$ are ordinary and pressure diffusion; assuming an ideal-gas behaviour for the solution, it may be shown, using equation (18.4–15) of Bird *et al.* (1960, p. 568), that

$$\mathbf{j}_A^* = -\mathbf{j}_B^* = -\rho^* D_{AB} \nabla^* \omega_A - \frac{(M_B - M_A) D_{AB}}{R_u T^*} \omega_A (1-\omega_A) \nabla^* p^*. \tag{3.3}$$

Here D_{AB} is the mass-diffusion coefficient, M_A and M_B are the molecular weights of species A and B respectively, R_u is the universal gas constant, p^* and T^* are the pressure and temperature of the gas respectively, and $\omega_A = \rho_A^*/\rho^*$ is the mass fraction of species A. Note that the first term on the left-hand side of (3.3) is the ordinary diffusion term in which the driving potential is local concentration gradient and which is modelled by Fick's law; the second term is a pressure-diffusion term in which the driving potential is the pressure gradient. A brief derivation of (3.3) is also given by Landau & Lifshitz (1959, p. 222) on the basis of kinetic theory.

For steady-flow conditions and for no chemical reactions within the centrifuge, it follows that (Bird *et al.* 1960, p. 555)

$$\nabla^* . \mathbf{n}_A^* = 0. \tag{3.4}$$

Using (3.2) and (3.3) and the dimensionless variables of §2, (3.4) may be written

$$\rho_e(r) E^{-\frac{1}{2}} (\mathbf{q} . \nabla) \omega_A - \delta \epsilon M^2 H(\omega_A) = \delta \nabla^2 \omega_A. \tag{3.5}$$

Here

$$H(\omega_A) = 2\omega_A(1-\omega_A) + r \frac{\partial}{\partial r} \{\omega_A (1-\omega_A)\}. \tag{3.6}$$

The two dimensionless parameters δ and ϵ are given by

$$\delta = \frac{E^{\frac{1}{2}}}{Sc\, \epsilon_f}, \quad \epsilon = \frac{M_B - M_A}{M_B}, \tag{3.7}$$

and M is the rotational Mach number defined in (2.3); the Schmidt number $Sc = \mu/\rho^* D_{AB}$ is assumed to be $O(1)$ and constant; E and ϵ_f are the Ekman and Rossby numbers defined in (2.7) and (2.9). In obtaining (3.5), it has been assumed

that both species A and B have large molecular weights and that $M_B > M_A$; the number-mean molecular weight $\overline{M}$ is given by

$$\frac{1}{\overline{M}} = \frac{1}{M_B} - \frac{\omega_A \epsilon}{M_A},$$

and in this study ϵ is assumed small; thus to leading order $\overline{M} \approx M_B$, and this result has been used to obtain (3.5). The neglected terms in (3.5) are $O(\delta\epsilon_f, \delta\epsilon M^2\epsilon_f, E^2/Sc\delta)$. It is also worthwhile to note that, according to the Chapman–Enskog kinetic theory, $\rho^* D_{AB}$ is a function of temperature alone (Bird *et al.* 1960, p. 510). In the present study, perturbations of the temperature field about the temperature of the bottom plate are small. Consequently $\rho^* D_{AB}$ is constant to leading order, and this result is used in obtaining (3.5).

The boundary conditions associated with (3.5) are that there is no normal mass flux through all solid walls, and, defining a dimensionless mass flux by $\mathbf{n}_A = \mathbf{n}_A^*/\rho_0^* U_1$, this condition is

$$\mathbf{N} \cdot \mathbf{n}_A = 0, \tag{3.8}$$

where $\mathbf{N}$ is a unit vector normal to the solid wall; at a location where mass enters the container $\mathbf{N} \cdot \mathbf{n}_A$ will in general be known. At radial boundaries the radial mass flux is given by

$$n_{A,r} = -E^{\frac{1}{2}}\delta\left\{\frac{\partial \omega_A}{\partial r} + \epsilon M^2 r_0 \omega_A(1-\omega_A)\right\} + \rho_e(r)\,\omega_A\, u, \tag{3.9}$$

where $r_0 = a$ or b, and u is the dimensionless radial velocity; at horizontal boundaries ($z_0 = 0$ or 1) the vertical mass flux is given by

$$n_{A,z} = -E^{\frac{1}{2}}\delta\frac{\partial \omega_A}{\partial z} + \rho_e\,\omega_A\, w, \tag{3.10}$$

where w is the vertical velocity. In general $n_{A,r} = 0$ at $r = r_0$ and $n_{A,z} = 0$ at $z = z_0$ for a solid wall.

Previously published studies on the mass transfer within gas centrifuges have been reviewed by Olander (1972) and more recently by Soubbaramayer (1979); generally some type of approximation for the fluid velocities is made in these studies and then a radially averaged solution to the mass-transfer problem (equation (40) of Olander 1972) is calculated. Commonly no attempt is made to analyse the interaction between the main core and the boundary-layer flows. For these and other reasons, the previous theoretical work on gas centrifuges is somewhat unsatisfying, and in this section a rational asymptotic analysis of the mass-transfer problem is considered. To establish the character of the solutions of (3.5) for a wide range of the parameter δ, it is convenient to assign a terminology to each parameter range and these are: (i) weak forced flow corresponding to $\epsilon_f \ll E^{\frac{1}{2}}$, $\delta \gg 1$; (ii) moderate forced flow corresponding to $\epsilon_f = O(E^{\frac{1}{2}})$, $\delta = O(1)$; and (iii) strong forced flow with $E^{\frac{1}{2}} \ll \epsilon_f \ll E^{\frac{1}{4}}$, $\delta \ll 1$. In this paper, the parameter ranges $\delta = O(1)$ and $\delta \ll 1$ will be investigated; the results of the case of weak forced flow, $\delta \gg 1$, will be reported elsewhere. The interaction of the fluid-mechanical boundary layers with the mass-transfer problem is a crucial feature of the separation process. This interaction is the subject of the analysis of §3.2.

3.2. *Boundary conditions*

Consider the model centrifuge depicted schematically in figure 1 for which the binary gas mixture enters the container at $r = a, z = 0$ with a unit (dimensionless) volumetric flow rate; let ω_{E} denote the mass fraction of the desirable (and assumed lighter) species A at the entrance port. Also denote the mass fraction of species A at the product port at $r = a$, $z = 1$ and at the waste port at $r = b$, $z = 0$ by ω_{P} and ω_{W} respectively. The cut θ is defined to be the ratio of the volumetric flow rate at the product port to that at the entrance port (Olander 1972). It is easily shown by requiring global species conservation that

$$\omega_{\mathrm{E}} = (1-\theta)\omega_{\mathrm{W}} + \theta\omega_{\mathrm{P}}. \tag{3.11}$$

One goal of centrifuge design is to maximize $\omega_{\mathrm{P}}/\omega_{\mathrm{E}}$ for sufficiently large throughput.

To develop the correct boundary conditions for the mass-transfer problem, consider first the geostrophic interior of the centrifuge. It has been demonstrated in §2 that, for either a thermally or mechanically driven centrifuge, the radial velocity $u = O(E)$ and the vertical velocity $w = O(E^{\frac{1}{2}})$ within the core. Let ω_0 be the $O(1)$ first term in an expansion of ω_A in powers of $E^{\frac{1}{2}}$ in the core; then it may be shown using (2.27) and (3.5) that

$$\rho_{\mathrm{e}}(r)\, W_{\mathrm{G}}(r) \frac{\partial \omega_0}{\partial z} - \frac{\delta \epsilon M^2}{r} \frac{\partial}{\partial r}\{r^2 \omega_0 (1-\omega_0)\} = \delta \nabla^2 \omega_0. \tag{3.12}$$

The solution of (3.12) must be carefully matched to the solutions of (3.5) in the velocity boundary layers.

Consider the Ekman layer near $z = 0$ for which the scaled vertical coordinate is $\zeta = \sigma^{\frac{1}{4}}(\rho_{\mathrm{e}}(r)/E)^{\frac{1}{2}} z$, where σ is defined in (2.30); substitution in (3.5) leads to

$$\frac{\partial^2 \omega_A}{\partial \zeta^2} = \frac{E^{\frac{1}{2}}}{\delta \sigma^{\frac{1}{2}}} (\mathbf{q} \,.\, \nabla)\, \omega_A + O\left(E, \frac{E}{\delta}, \epsilon E\right), \tag{3.13}$$

where $\mathbf{q}$ is the dimensionless velocity in the Ekman layer. This equation suggests that the asymptotic expansion of ω_A in the Ekman layer is

$$\omega_A = \bar{\omega}_0(r, \zeta) + \frac{E^{\frac{1}{2}}}{\delta \sigma^{\frac{1}{2}}} \bar{\omega}_1(r, \zeta) + \ldots, \tag{3.14}$$

where the series is indeed asymptotic, and the error terms in (3.13) are small, only if $E^{\frac{1}{2}} \ll \delta \ll E^{-\frac{1}{2}}$; substitution of (3.14) into (3.13) gives

$$\frac{\partial^2 \bar{\omega}_0}{\partial \zeta^2} = 0, \quad \frac{\partial^2 \bar{\omega}_1}{\partial \zeta^2} = (\mathbf{q} \,.\, \nabla)\, \bar{\omega}_0. \tag{3.15a, b}$$

The boundary conditions are obtained by substitution of (3.14) in (3.10) and requiring that the species flux $n_{A,z}$ vanish at $\zeta = 0$; this leads to

$$\frac{\partial \bar{\omega}_0}{\partial \zeta} = \frac{\partial \bar{\omega}_1}{\partial \zeta} = 0 \quad \text{at} \quad \zeta = 0. \tag{3.16}$$

The solution of (3.15a) that satisfies the condition (3.16) and that matches smoothly into the geostrophic solution is

$$\bar{\omega}_0 = \omega_0(r, 0), \tag{3.17}$$

and consequently the species mass fraction is invariant to leading order across the Ekman layer. The solution of (3.15b) satisfying (3.16) is

$$\bar{\omega}_1 = C_1(r) + \left.\frac{\partial \omega_0}{\partial r}\right|_{z=0} \int_0^{\zeta} (\zeta - t)\, \bar{u}(r, t)\, dt. \tag{3.18}$$

Here $\bar{u}(r, \zeta)$ is the radial velocity in the Ekman layer and C_1 is an arbitrary function of r. The asymptotic form of (3.18) is easily found to be

$$\omega_1 \sim \left.\frac{\partial \omega_0}{\partial r}\right|_{z=0} \sigma^{\frac{1}{4}} \rho_e^{\frac{1}{2}} \zeta \mathscr{F}_{\frac{1}{2}}(r, 0) \text{ as } \zeta \to \infty, \tag{3.19}$$

where

$$\mathscr{F}_{\frac{1}{2}}(r, 0) = E^{-\frac{1}{2}} \int_0^\infty \bar{u} \, dz \tag{3.20}$$

is the magnitude of the $O(E^{\frac{1}{2}})$ volumetric flow rate per unit length of circumference in the lower Ekman layer; this quantity is given explicitly in (2.105). Expanding $\omega_0(r, z)$ in a Taylor series about $z = 0$ and matching (3.14) leads to the boundary condition on the core solution $\omega_0(r, z)$ as $z \to 0$. A similar procedure may be easily carried out for the upper Ekman layer, and the generalization is

$$\mp \rho_e \mathscr{F}_{\frac{1}{2}}(r, z_0) \frac{\partial \omega_0}{\partial r} = \delta \frac{\partial \omega_0}{\partial z} \quad \text{at} \quad z = z_0 = \tfrac{1}{2} \pm \tfrac{1}{2}. \tag{3.21}$$

Here $\mathscr{F}_{\frac{1}{2}}(r, 1)$ represents the volumetric flow rate in the $+r$-direction per unit length of circumference in the upper Ekman layer.

To obtain the boundary conditions for $\omega_0(r, z)$ at the sidewalls, consider first the $E^{\frac{1}{3}}$ layer, for which the scaled radial variable is $\eta = \rho_e^{\frac{1}{3}}(r_0) \sigma^{\frac{1}{6}}(r_0) \beta (r - r_0) E^{-\frac{1}{3}}$; here $r_0 = a$ or b, and $\beta = +1$ at $r_0 = a$ and $\beta = -1$ at $r_0 = b$. The expansions for the velocity components in the $E^{\frac{1}{3}}$ layer are given in (2.86)–(2.88), and upon substitution it may be shown that the leading-order terms in (3.5) are given by

$$\frac{\partial^2 \omega_A}{\partial \eta^2} = -\frac{E^{\frac{1}{3}}}{\delta} \rho_e^{\frac{1}{6}} \sigma^{\frac{1}{12}} \beta \, V_G(r_0) \left\{ u_2 \frac{\partial \omega_A}{\partial \eta} + w_2 \frac{\partial \omega_A}{\partial z} \right\} + \frac{\epsilon M^2 r_0}{\rho_e^{\frac{1}{3}} \sigma^{\frac{1}{6}}} \beta E^{\frac{1}{3}} \frac{\partial}{\partial \eta} \{\omega_A (1 - \omega_A)\}, \tag{3.22}$$

and the form of this equation suggests an expansion in the $E^{\frac{1}{3}}$ layer of the form

$$\omega_A = \tilde{\omega}_0(\eta, z) + \frac{E^{\frac{1}{3}}}{\delta} \rho_e^{\frac{1}{6}} \sigma^{\frac{1}{12}} \beta V_G(r_0) \tilde{\omega}_1(\eta, z) + \ldots. \tag{3.23}$$

Here $V_G(r_0)$ is the geostrophic azimuthal velocity associated with either a thermally or a mechanically driven centrifuge evaluated as $r \to r_0$. The usual limit process ($E \to 0$, η fixed) applied to (3.22) leads to

$$\frac{\partial^2 \tilde{\omega}_0}{\partial \eta^2} = 0. \tag{3.24}$$

The solid-wall condition is obtained by setting $n_{A,r} = 0$ in (3.9), and this requires that $\partial \tilde{\omega}_0 / \partial \eta$ vanish at $\eta = 0$; the solution of (3.24) satisfying this condition is

$$\tilde{\omega}_0 = A_0(z), \tag{3.25}$$

where $A_0(z)$ is at this stage an arbitrary function of z. The equation satisfied by $\tilde{\omega}_1$ is obtained by substitution of (3.23) into (3.22), and it is easily shown that

$$\frac{\partial^2 \tilde{\omega}_1}{\partial \eta^2} = -w_2(\eta, z) A_0'(z), \tag{3.26}$$

with the boundary condition (obtained from (3.9)) that

$$\frac{\partial \tilde{w}_1}{\partial \eta} = -\delta \epsilon M^2 r_0 A_0(z) \{1 - A_0(z)\} \quad \text{at} \quad \eta = 0. \tag{3.27}$$

Here ρ_e and σ are evaluated at $r = r_0$. The solution of (3.26) satisfying (3.27) is

$$\tilde{\omega}_1(\eta, z) = B_0(z) - A_0'(z)\int_0^\eta (\eta - t)\, w_2(t, z)\, dt - \frac{\delta\epsilon M^2 r_0 A_0(1-A_0)\eta}{\rho_e^{\frac{1}{2}}\sigma^{\frac{1}{4}} V_G(r_0)}, \tag{3.28}$$

where $B_0(z)$ is an arbitrary function of z. Note that, in order for the terms neglected in obtaining (3.22) to be small and in order for the series (3.23) to be truly asymptotic, it may be shown that δ is restricted to the parameter range $E^{\frac{1}{3}} \ll \delta \ll E^{-\frac{1}{3}}$.

As $\eta \to \infty$, the series (3.23) must match the solution in the $E^{\frac{1}{4}}$ layer; upon examining the form of (3.28) for large η and expressing η in terms of the $E^{\frac{1}{4}}$ layer variable $\xi = \sqrt{2}\,\sigma^{\frac{1}{8}}\rho_e^{\frac{1}{4}}\beta(r - r_0)E^{-\frac{1}{4}}$ according to $\eta = \sqrt{\frac{1}{2}}\xi\rho_e^{\frac{1}{12}}\sigma^{\frac{1}{24}}E^{\frac{1}{12}}$, (3.23) becomes

$$\omega_A = A_0(z) + \frac{\beta E^{\frac{1}{4}}\rho_e^{\frac{3}{4}}}{\sqrt{2}\,\delta\sigma^{\frac{1}{8}}}\left\{\beta\mathscr{F}_{\frac{1}{3}}A_0' - \frac{\delta\epsilon M^2 r_0 A_0(1-A_0)}{\rho_e}\right\}\xi + \ldots. \tag{3.29}$$

Here ρ_e and σ are evaluated at $r = r_0$, and $\mathscr{F}_{\frac{1}{3}}$ is the magnitude of the $O(E^{\frac{1}{2}})$ volumetric flux in the $E^{\frac{1}{3}}$ layer per unit length of circumference in the positive z-direction, defined by

$$\mathscr{F}_{\frac{1}{3}}(r_0) = E^{-\frac{1}{2}}\int_0^\infty w_{\frac{1}{3}}\,|dr|\,. \tag{3.30}$$

This quantity is evaluated in (2.107).

The form of (3.29) suggests an expansion in the $E^{\frac{1}{4}}$ layer,

$$\omega_A = \Omega_0(\xi, z) + \frac{\beta E^{\frac{1}{4}}\rho_e^{\frac{1}{4}}}{\sqrt{2}\,\delta}\,\sigma^{\frac{1}{8}}\Omega_1(\xi, z) + \ldots, \tag{3.31}$$

and, upon substitution in (3.5) along with the $E^{\frac{1}{4}}$ layer velocity expansions given in (2.67), the lowest-order equations

$$\frac{\partial^2\Omega_0}{\partial\xi^2} = 0, \quad \frac{\partial^2\Omega_1}{\partial\xi^2} = W(\xi, z)\frac{\partial\Omega_0}{\partial z} \tag{3.32}$$

are obtained, where $W(\xi, z)$ is the magnitude of the $O(E^{\frac{1}{4}})$ vertical velocity in the $E^{\frac{1}{4}}$ layer. The boundary conditions as $\xi \to 0$ are obtained by substituting the expansions (3.23) and (3.31) into (3.9) and matching in the limits $\xi \to 0$, $\eta \to \infty$; this is equivalent to requiring that (3.31) behave according to (3.29) for small ξ, and leads to

$$\frac{\partial\Omega_0}{\partial\xi} = 0, \quad \rho_e^{\frac{1}{2}}\sigma^{\frac{1}{4}}\frac{\partial\Omega_1}{\partial\xi} = -\delta\epsilon M^2 r_0 A_0(1-A_0) + \beta\rho_e\mathscr{F}_{\frac{1}{3}}A_0', \tag{3.33}$$

at $\xi = 0$. Again ρ_e and σ are evaluated at $r = r_0$. The solutions of (3.32) satisfying (3.33) are

$$\Omega_0(\xi, z) = A_0(z), \tag{3.34}$$

$$\Omega_1(\xi, z) = A_0'(z)\int_0^\xi (\xi - t)\, W(t, z)\, dt + \frac{\xi}{\sigma^{\frac{1}{4}}\rho_e^{\frac{1}{2}}}\{\beta\rho_e\mathscr{F}_{\frac{1}{3}}A_0'(z) - \delta\epsilon M^2 r_0 A_0(1-A_0)\}. \tag{3.35}$$

Note that it may be shown that, for the terms neglected in obtaining (3.32) to be of lower relative order and in order for the expansion (3.31) to be truly asymptotic, δ is restricted to the parameter range $E^{\frac{1}{4}} \ll \delta \ll E^{-\frac{1}{4}}$.

Matching to the geostrophic region is carried out by taking the limit for large ξ in (3.31) and (3.25) and by expanding $\omega_0(r, z)$ in a Taylor series about $r = r_0$; the matching leads to

$$A_0(z) = \omega_0(r_0, z), \tag{3.36}$$

$$\beta\rho_e(r_0)\mathscr{F}_s(r_0)\frac{\partial\omega_0}{\partial z} - \epsilon\delta r_0 M^2\omega_0(1-\omega_0) = \delta\frac{\partial\omega_0}{\partial r} \tag{3.37}$$

at $r = r_0$; here again, for $r_0 = a$, $\beta = 1$ and for $r_0 = b$, $\beta = -1$. The quantity $\mathscr{F}_s(r_0)$ denotes the total volumetric flow rate in the Stewartson layers, and

$$\mathscr{F}_s(r_0) = \mathscr{F}_{\frac{1}{4}}(r_0) + \mathscr{F}_{\frac{1}{3}}(r_0), \tag{3.38}$$

where $\mathscr{F}_{\frac{1}{3}}(r_0)$ is defined by (3.30); $\mathscr{F}_{\frac{1}{4}}(r_0)$ is the magnitude of the $O(E^{\frac{1}{2}})$ volumetric flow rate in the $E^{\frac{1}{4}}$ layer in the positive z-direction per unit length of circumference, defined according to

$$\mathscr{F}_{\frac{1}{4}}(r_0) = E^{-\frac{1}{2}} \int_0^\infty w_{\frac{1}{4}} |dr| . \tag{3.39}$$

The boundary conditions for the geostrophic mass-fraction distribution are thus given by (3.21) and (3.37); however, for $\epsilon M^2 \ll 1$ the nonlinear term in (3.37) is negligible and the boundary conditions contain only first derivatives. In this case the solution to (3.12) is only unique to within an additive constant; to pose the problem uniquely requires appending the condition (for the model centrifuge)

$$\omega_0 = \omega_E \quad \text{at} \quad z = 0, \quad r = a. \tag{3.40}$$

Note that the condition (3.11) need not be specified; it may be demonstrated by integration of (3.12) over the entire domain using the boundary conditions (3.21), (3.37) and (3.40) that the condition (3.17) is identically satisfied.

For the model centrifuge depicted in cross-section in figure 1, the vertical drift velocity in the core is $O(E^{\frac{1}{2}})$; the magnitude has been computed in §2 and is

$$W_G(r) = \frac{q}{4r\rho_e(r)} \frac{\partial}{\partial r} \left\{ \frac{r^2 \rho_e^{\frac{1}{2}}(r)}{\sigma^{\frac{3}{4}}} \right\}. \tag{3.41}$$

Here q is a constant related to the magnitude of differential rotation of the top and bottom plates and the amount of differential heating between the end plates; in particular (see (2.23) and (2.26))

$$q = \lambda_m(\lambda_1 - \lambda_0) - \tfrac{1}{2}\lambda_T. \tag{3.42}$$

Finally, for the model centrifuge the volumetric fluxes may be evaluated using the results of §2, and these are

$$\mathscr{F}_{\frac{1}{2}}(r, z_0) = \frac{1}{2} \left\{ \frac{(1-\theta)a}{\rho_e(r)} \pm \frac{1}{2} \frac{qr}{\sigma^{\frac{3}{4}} \rho_e^{\frac{1}{2}}} \right\} \quad \text{at} \quad z_0 = \tfrac{1}{2} \pm \tfrac{1}{2}, \tag{3.43}$$

$$\mathscr{F}_s(r_0) = \frac{(\theta \pm 1)a}{2r_0 \rho_e(r_0)} \pm \frac{qr_0}{4\sigma^{\frac{3}{4}} \rho_e^{\frac{1}{2}}} \quad \text{at} \quad r_0 = \tfrac{1}{2}(a+b) \mp \tfrac{1}{2}(b-a). \tag{3.44}$$

These results will now be used in §§ 3.3 and 3.4 to examine solutions to the mass transfer problem for the model centrifuge.

3.3. *The core mass-fraction distribution for $\delta = O(1)$*

In this section, the solution of (3.12) subject to the boundary conditions (3.21), (3.37) and (3.40) will be computed for the case $\delta = O(1)$ for the model centrifuge; physically this parameter range corresponds to the case of moderately forced flow in the sense that (from (3.7)) the fluid Rossby number $\epsilon_f = O(E^{\frac{1}{2}})$. It is assumed that $\epsilon M^2 \ll 1$, and from (3.12) an expansion of the form

$$\omega_A = \omega_E + \epsilon M^2 \omega_E (1 - \omega_E)\, \omega + \ldots, \tag{3.45}$$

is suggested, where ω_E is the mass fraction of species A at the entrance port. The

perturbation term ω satisfies

$$\nabla^2\omega = -2 + \frac{\rho_E(r)}{\delta} W_G(r) \frac{\partial \omega}{\partial z}, \tag{3.46}$$

and the boundary conditions are

$$\pm\rho_e(r)\,\mathscr{F}_{\frac{1}{2}}(r, z_0)\frac{\partial \omega}{\partial r} = \delta \frac{\partial \omega}{\partial z} \text{at} \quad z_0 = \tfrac{1}{2} \mp \tfrac{1}{2}, \tag{3.47}$$

$$\pm\rho_e(r_0)\,\mathscr{F}_s(r_0)\frac{\partial \omega}{\partial z} - \delta r_0 = \delta \frac{\partial \omega}{\partial r} \quad \text{at} \quad r_0 = \tfrac{1}{2}(a+b) \pm \tfrac{1}{2}(a-b), \tag{3.48}$$

$$\omega = 0 \quad \text{at} \quad r = a,\ z = 0. \tag{3.49}$$

This linear boundary-value problem is difficult to solve owing to the complexity of the boundary conditions and the fact that the Ekman-layer fluxes in (3.47) and the vertical drift velocity in (3.46) are non-trivial functions of r; consequently a closed-form analytical solution is not readily available and solutions were obtained numerically using finite-difference methods. The numerical scheme is described in the appendix.

Calculations were carred out for a binary gas having a Prandtl number $Pr = 1$ and a ratio of specific heats $\gamma = 1{\cdot}05$; in addition, a value of the parameter $\delta = 1$ was used. A number of different rotational Mach numbers $O(1)$ were considered as well as differing values of the cut θ and the inner and outer dimensionless radii a and b respectively. In the calculations discussed in this section the parameter q (defined in (3.42)) was taken equal to zero, and consequently mass-fraction distributions were obtained in this parameter range for a purely source–sink flow only. In order to ensure an accurate solution, calculations were normally carried out with 3 mesh sizes. For $a = 1$, $b = 2$, for example, 11 points, then 21 points and finally 41 points in each direction were employed; generally, for lower values of M, excellent agreement between successive solutions was obtained in this way. Typically several-hundred iterations were required for convergence.

Some selected results are plotted in figures 2 and 3. In figure 2, lines of constant scaled mass fraction ω are plotted for a pure source–sink flow. Note the sourcelike level curves in the vicinity of the entrance port at $r = a$, $z = 0$, which is suggestive of an irregular behaviour in ω at the corner; this is supported in the calculations, where it was observed that good agreement between successive solutions was hardest to achieve in the corner regions. However, it was observed in the calculations that the influence of the irregularity is largely confined to the corner region. The increasing enrichment toward the product corner should be noted, as well as the progressive depletion toward the outer wall.

A separation or enrichment factor is defined by $\alpha = \omega_P/\omega_E$, and a scaled separation factor is plotted in figure 3 as a function of the cut θ for various geometries; the data points on figure 3 represent the results of numerical calculations for $q = 0$ with the rotational Mach number held fixed at $M = 1$ and the outer radius held fixed at $b = 1$. It is evident from figure 3 that, for a fixed value of $\delta\epsilon M^2(1-\omega_E)$, the scaled separation factor $(\alpha-1)/\{\delta\epsilon M^2\omega_E(1-\omega_E)\}$ is nearly a linearly decreasing function of the cut; this variation is typical of centrifuge operation (Olander 1972). In addition, it may be observed that a 'fatter' centrifuge (smaller inner radius a) leads to better enrichment for the model centrifuge. Several additional calculations were also carried out for different rotational Mach numbers M; these calculations indicate a linear increase in the parameter $(\alpha-1)/\{\delta\epsilon(1-\omega_E)\}$ with M^2. Consequently enrichment in this parameter

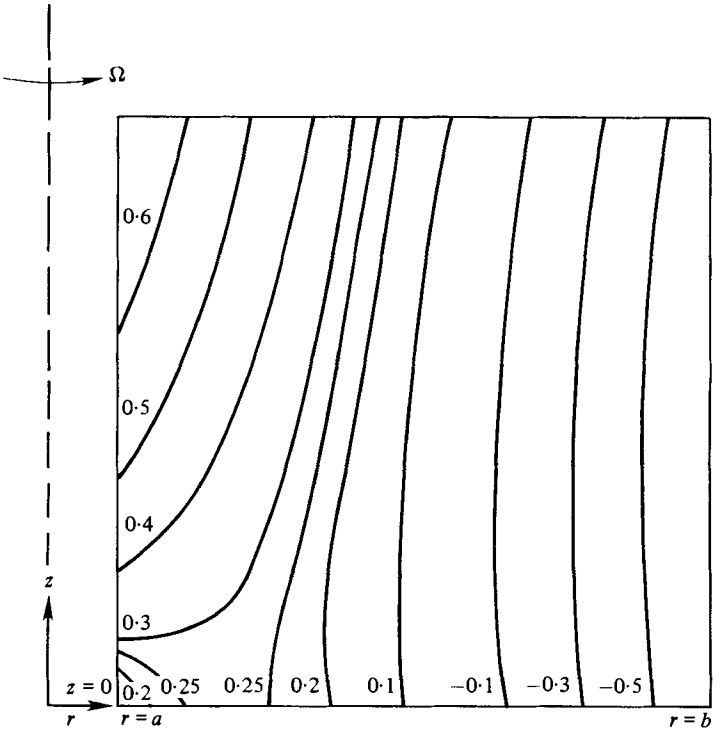

FIGURE 2. Isomass-fraction lines for $M = 1$. Here $a = 1$, $b = 2$, the cut $\theta = 0{\cdot}5$, and there is a pure source–sink flow, $f = 0$. Numbers next to the curves indicate values of the scaled mass fraction $\omega = (\omega_A - \omega_E)/(\epsilon M^2 \omega_E(1 - \omega_E))$.

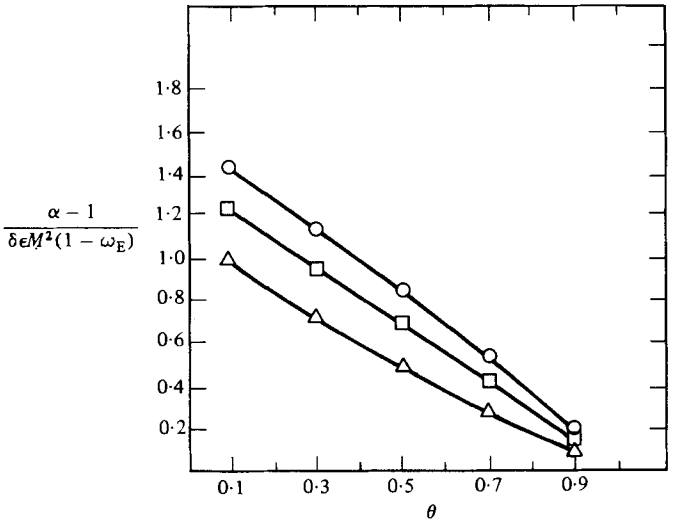

FIGURE 3. Scaled separation factor as a function of the cut for several geometries. Here $M = 1$, $b = 2$. △, $a = 1{\cdot}5$; □, 1·0; ○, 0·5. Here $q = 0$.

range is also enhanced by increased rotation rates which again is consistent with observed trends (Olander 1972).

3.4. *The mass-fraction distribution for small* δ

In this section, a singular perturbation solution is developed for the mass-fraction distribution for the case $\delta \to 0$. It may be observed from (3.7) that $\delta \ll 1$ implies that $\epsilon_f \gg E^{\frac{1}{2}}$; consequently the centrifuge throughput must be relatively high, and this parameter range is referred to as the strong-forced-flow case. For the analysis in §3.2 to be valid, $\delta \gg E^{\frac{1}{4}}$, and therefore the parameter range of interest here is

$$E^{\frac{1}{4}} \ll \delta \ll 1, \quad E^{\frac{1}{4}} \gg \epsilon_f \gg E^{\frac{1}{2}}. \tag{3.50a, b}$$

In addition it is assumed that ϵM^2 is $O(1)$ in the limit process $\delta, E \to 0$. In this physical regime, the structure consists of a core distribution with concentration boundary layers having a thickness $O(\delta^{\frac{1}{2}})$ on $r = a+$ and $r = b-$. For $W_G > 0$, a concentration layer of width $O(\delta)$ exists on $z = 1-$, while for $W_G < 0$ the horizontal layer occurs at $z = 0+$. Note that, by virtue of (3.50a), both types of concentration boundary layers are thicker than any of the velocity boundary layers.

In the core of the centrifuge, the following expansion is assumed for the mass fraction of species A:

$$\omega_A = \omega_E + \delta\epsilon M^2 \omega_E (1-\omega_E)\, \omega_1(r, z) + \ldots, \tag{3.51}$$

where ω_E is the value of ω_A at the entrance port. Substitution in (3.12) gives the leading-order equation

$$\rho_e(r)\, W_G(r) \frac{\partial \omega_1}{\partial z} = 2. \tag{3.52}$$

It is convenient to define a constant s by

$$s = \operatorname{sgn}\{W_G(r)\}, \tag{3.53}$$

and substitution of (3.51) in the boundary condition (3.21) gives

$$\frac{\partial \omega_1}{\partial r} = 0 \quad \text{on} \quad z = \tfrac{1}{2}(1-s). \tag{3.54}$$

The solution is

$$\omega_1 = C + \frac{2}{\rho_e(r)\, W_G(r)} \{z - \tfrac{1}{2}(1-s)\}, \tag{3.55}$$

where C is a constant to be determined.

The sidewall concentration layers are considered next, and define a boundary-layer variable $y = \beta(r - r_0)\, \delta^{-\frac{1}{2}}$, where $\beta = 1$ for $r_0 = a$ and $\beta = -1$ for $r_0 = b$. Assuming the expansion

$$\omega_A = \omega_E + \delta\epsilon M^2 \omega_E (1-\omega_E)\, \tilde{\omega}_1(y, z) + \ldots, \tag{3.56}$$

it may be shown that

$$\rho_e(r_0)\, W_G(r_0) \frac{\partial \tilde{\omega}_1}{\partial z} - \frac{\partial^2 \tilde{\omega}_1}{\partial y^2} = 2; \tag{3.57}$$

the boundary condition at $y = 0$ follows from (3.37), and is

$$\frac{\partial \tilde{\omega}_1}{\partial z} = \frac{\beta r_0}{\rho_e(r_0)\, \mathscr{F}_s(r_0)} \quad \text{at} \quad y = 0. \tag{3.58}$$

This equation may be integrated to obtain

$$\tilde{\omega}_1 = \frac{\beta r_0 z}{\rho_e(r_0)\, \mathscr{F}_s(r_0)} + C' \quad \text{at} \quad y = 0, \tag{3.59}$$

where C' is a constant.

Consider now the concentration layer at $r = a+$; since $\omega_A = \omega_E$ at $r = a, z = 0$ then $C' = 0$. The solution of (3.57) that satisfies (3.59) and matches (3.55) as $y \to \infty$ is given by

$$\tilde{\omega}_1(y, z) = \frac{2z}{\rho_e(a)\, W_G(a)} - D_0\{z - \tfrac{1}{2}(1-s)\}\left\{(2\zeta^2+1)\operatorname{erfc}\zeta - \frac{2}{\sqrt{\pi}}\zeta e^{-\zeta^2}\right\} + (C+D_1)\operatorname{erf}\zeta + D_2, \quad (3.60)$$

where the constants D_0, D_1 and D_2 are

$$D_0 = \frac{2}{W_G(a)} - \frac{a}{\mathscr{F}_s(a)}, \quad D_1 = \frac{a(s-1)}{2\mathscr{F}_s(a)}, \quad D_2 = \tfrac{1}{2}(s-1)\, D_0, \quad (3.61)$$

and the variable ζ is defined by

$$\zeta = \frac{y}{2}\left\{\frac{\rho_e(a)\, W_G(a)}{z - \tfrac{1}{2}(1-s)}\right\}^{\frac{1}{2}}. \quad (3.62)$$

This solution describes a boundary layer that originates at the corner $r = a$, $z = \frac{1}{2}(1-s)$ and thickens along $r = a$ towards the other horizontal wall. The value of $\tilde{\omega}_1$ at the product port is given by

$$\tilde{\omega}_1(a, 1) = \frac{a}{\mathscr{F}_s(a)}, \quad (3.63)$$

and using (3.59), together with the global species-conservation result in (3.11), the variation for the boundary-layer function on $r = b$ may be shown to be

$$\tilde{\omega}_1(0, z) = \frac{-bz}{\rho_e(b)\, \mathscr{F}_s(b)} - \frac{\theta a}{(1-\theta)\, \mathscr{F}_s(a)}. \quad (3.64)$$

This is the boundary condition at $y = 0$ for the calculation of the concentration-layer solution near $r = b$. This solution is given by replacing a by b in (3.60) and (3.62) and by replacing the constants D_0, D_1, D_2 by

$$D_0' = \frac{1}{\rho_e(b)}\left\{\frac{2}{W_G(b)} + \frac{b}{\mathscr{F}_s(b)}\right\},$$

$$D_1' = -\frac{(s-1)\, b}{2\rho_e(b)\, \mathscr{F}_s(b)} + \frac{\theta a}{(1-\theta)\, \mathscr{F}_s(a)},$$

$$D_2' = \tfrac{1}{2}(s-1)\, D_0' - \frac{\theta a}{(1-\theta)\, \mathscr{F}_s(a)} \quad (3.65)$$

respectively.

A horizontal boundary layer is required at $z = \frac{1}{2}(s+1)$; defining a boundary-layer variable $\zeta' = -s(z - \frac{1}{2}(1+s))\,\delta^{-1}$ and an expansion according to

$$\omega_A = \omega_E + \delta\epsilon M^2 \omega_E(1-\omega_E)\,\bar{\omega}_1(r, \zeta') + \ldots, \quad (3.66)$$

the leading-order form for (3.12) is

$$\frac{\partial^2 \bar{\omega}_1}{\partial \zeta'^2} = -s\rho_e(r)\, W_G(r)\frac{\partial \bar{\omega}_1}{\partial \zeta'}. \quad (3.67)$$

The boundary condition at $\zeta' = 0$ is obtained from (3.21) and

$$\frac{\partial \bar{\omega}_1}{\partial \zeta'} = \rho_e(r)\, \mathscr{F}_{\frac{1}{2}}(r, \tfrac{1}{2}(s+1))\frac{\partial \bar{\omega}_1}{\partial r} \quad \text{at} \quad \zeta' = 0, \quad (3.68)$$

while matching to the core solution (3.55) requires that

$$\bar{\omega}_1 \sim C + \frac{2s}{\rho_e(r)\, W_G(r)} \quad \text{as} \quad \zeta' \to \infty. \tag{3.69}$$

The solution is given by

$$\bar{\omega}_1(r, \zeta') = C + \frac{2s}{\rho_e(r)\, W_G(r)} + \left\{ \frac{-2s}{\rho_e(r)\, W_G(r)} + \frac{(D + r^2)}{r\rho_e(r)\, \mathscr{F}_{\frac{1}{2}}(r, \frac{1}{2}(s+1))} \right\} \exp\left(-s\rho_e(r)\, W_G(r)\, \zeta'\right), \tag{3.70}$$

where D is another constant to be determined.

It may readily be shown by consideration of the extension of the $O(\delta)$ horizontal concentration layer under the $O(\delta^{\frac{1}{2}})$ sidewall layers that, for $s = 1$, the limit of (3.70) at $\zeta' = 0$, $r \to a$ must be equal to the limit of (3.60) at $\zeta = 0$, $z \to 1$. This gives a continuous solution in the corner $r = a+$, $z = 1-$; an analogous condition is applied in the corner $r = b-$, $z = 1-$. If $s = -1$, the sidewall concentration layers originate in the upper corners and grow toward $z = 0$; in this case continuity in the corners $(a, 0)$ and $(b, 0)$ is required. In either case these conditions determine values for the constants C and D in (3.70), and

$$C\{a\mathscr{F}_{\frac{1}{2}}(a, z_0) - b\rho_e(b)\, \mathscr{F}_{\frac{1}{2}}(b, z_0)\} = \frac{s+1}{2} \left\{ \frac{a^2 \mathscr{F}_{\frac{1}{2}}(a, z_0)}{\mathscr{F}_S(a)} + \frac{b^2 \mathscr{F}_{\frac{1}{2}}(b, z_0)}{\mathscr{F}_S(b)} \right\} + b^2 - a^2 + \frac{\theta ab}{1-\theta} \rho_e(b) \frac{\mathscr{F}_{\frac{1}{2}}(b, z_0)}{\mathscr{F}_S(a)}, \tag{3.71}$$

$$D = \frac{(s+1)\, a^2 \mathscr{F}_{\frac{1}{2}}(a, z_0)}{2\mathscr{F}_S(a)} - a^2 - a\mathscr{F}_{\frac{1}{2}}(a, z_0)\, C, \tag{3.72}$$

where $z_0 = \frac{1}{2}(s+1)$.

A self-consistent solution has been completed here for $E^{\frac{1}{4}} \ll \delta \ll E^{-\frac{1}{4}}$; in terms of the performance of the centrifuge, the principal result is the evaluation of the enrichment factor α from (3.63) and

$$\alpha = \frac{\omega_P}{\omega_E} = 1 + \frac{\delta\epsilon M^2 a(1 - \omega_E)}{\mathscr{F}_S(a)}, \tag{3.73}$$

where the flux in the sidewall boundary layer is given by (3.44) according to

$$\mathscr{F}_S(a) = \tfrac{1}{2}(\theta + 1) + \tfrac{1}{4} q (\sigma(a))^{-\frac{3}{4}}. \tag{3.74}$$

Note that $\mathscr{F}_S(a) = 0$ at $q = q_c$, where

$$q_c = -2(1 + \theta)\, (\sigma(a))^{\frac{3}{4}}, \tag{3.75}$$

and near this critical level of differential rotation and/or differential heating, (3.73) is not valid. In this situation the concentration-layer problem on $r = a$ must be re-examined. In particular, consider the case when $\mathscr{F}_S(a) = O(\delta^{\frac{1}{2}})$; it may be deduced from the boundary condition (3.37) that in this situation the perturbation in the centrifuge to the entering value ω_E is $O(\delta^{\frac{1}{2}})$ and that all terms in (3.37) are important to leading order on $r = a$. In addition, the expansions in the core region and boundary layers given by (3.51) and (3.56) must be modified to include an $O(\delta^{\frac{1}{2}})$ term. The boundary-layer structure is similar to the previous case, but the solutions are complex and are not included here.

As long as $\delta^{\frac{1}{2}}/\mathscr{F}_S(a)$ is $o(1)$, the solution (3.60) is correct, and it is of interest to examine the properties of the mass-fraction distribution in this parameter range. In

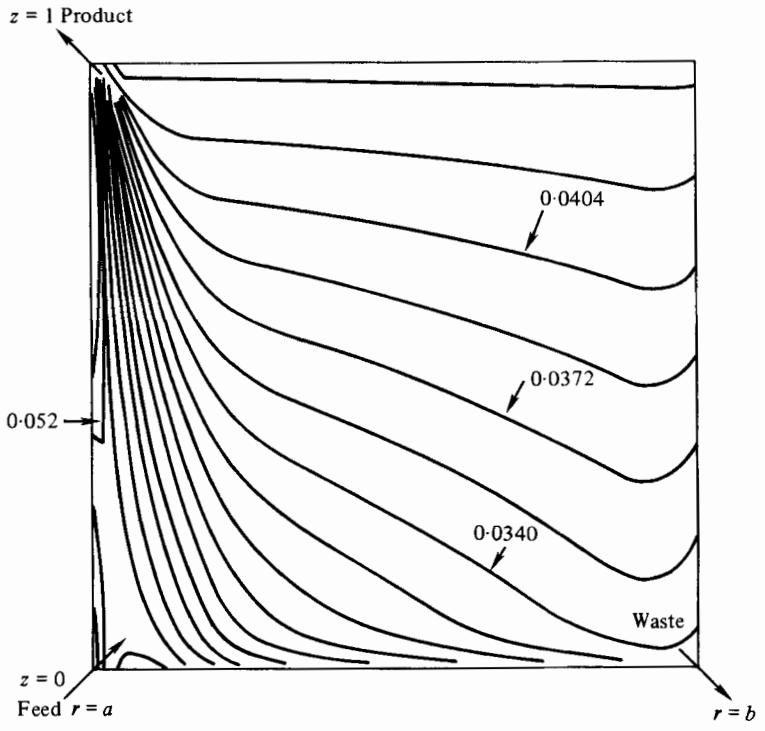

FIGURE 4. Isomass-fraction contours for ω_A for $q = -1$, $M = 1$, $a = 1$, $b = 2$, $\theta = 0{\cdot}5$ and $\epsilon = 0{\cdot}01$. Here $\omega_E = 0{\cdot}05$ and the boundary-layer regions are to scale for $\delta = 0{\cdot}02$. Contours for ω_A are at intervals of $1{\cdot}6 \times 10^{-3}$. Typical values of the mass fraction are indicated.

figure 4, absolute isomass-fraction contours are given for the case $\omega_E = 0{\cdot}05$, $\delta = 0{\cdot}02$ and $\epsilon = 0{\cdot}01$; in addition, the cut $\theta = 0{\cdot}5$ and $a = 1$, $b = 2$. The rotational Mach number $M = 1$, and there is a downward drift in the core region with $q = -1$; note that this value of q is close to, but greater than, the critical value given in (3.75). To prepare figure 4, a composite solution consisting of the core and boundary-layer concentration solutions was formed. Generally the values associated with each contour decrease radially outward in figure 4. Note the collection of contours near the product port; in addition the presence of the sidewall boundary layers as well as the endwall concentration layer at $z = 0$ is clearly demonstrated.

In figure 5, the scaled separation factor $(\alpha - 1)/\{\epsilon\delta a M^2(1 - \omega_E)\}$ is plotted as a function of the parameter q for various values of the inner radius a. Positive values of q correspond to the physical situation of an upward drift in the core induced by either differential rotation or differential heating, and in this case a net upward motion occurs in the velocity boundary layers at $r = a$. Enrichment always occurs for $q > 0$, and is essentially independent of the inner radius a as well as the value of the outer radius b. As q decreases, the enrichment process is enhanced and the separation factor increases to relatively large values, as the critical value of q given by (3.80) is approached. For $q < 0$, the induced drift in the core is downwards, but in the regime depicted in figure 5 the net motion in the sidewall velocity boundary layer at $r = a$ is still upwards. As $q \to q_c$ the flux in the boundary layer approaches zero. Note, in this parameter range, that separation is enhanced at smaller values of the inner radius a. For $q < q_c$, it may be inferred from (3.73) and (3.74) that the mixture becomes depleted in species A at the product port; in this regime, the vertical velocity in the

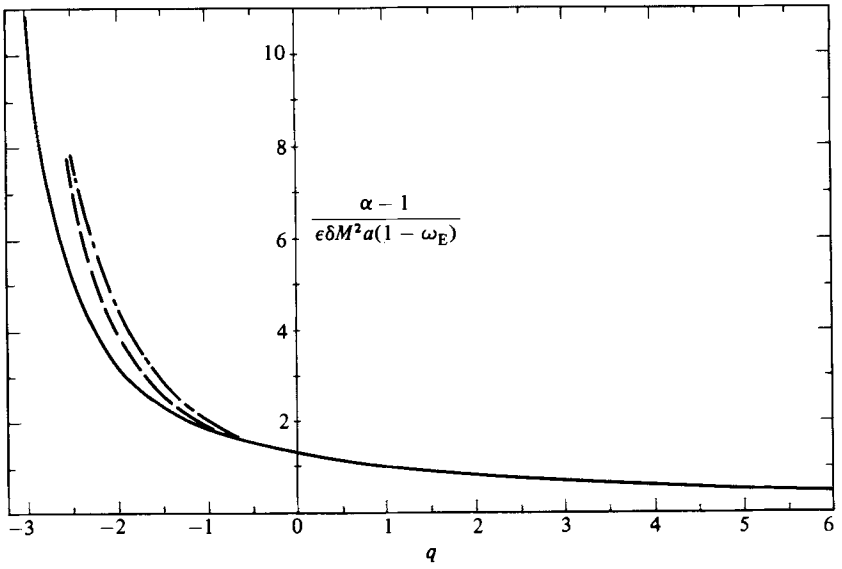

FIGURE 5. Enrichment for small δ versus q for $M = 1$, $\theta = 0{\cdot}5$ and various values of a: ——, $a = 2$; – – –, 1·5; — — —, 1. Note that the enrichment is independent of b.

boundary layers and the core is negative. The physical reason for this behaviour is as follows.

As the binary gas enters at the feed port it rises into the $E^{\frac{1}{3}}$ layer on $r = a$, and a portion moves radially outward toward the $E^{\frac{1}{4}}$ layer. As the gas enters the $E^{\frac{1}{4}}$ layer it is deflected toward the Ekman layers on the endwalls, whereupon the source–sink part of the flow moves outwards toward $r = b$. For $q < 0$, a recirculatory motion in a counter-clockwise direction is set up and superimposed on the source–sink flow. As the gas stream traverses the bottom Ekman layer, depletion of species A occurs and a portion of the gas stream is removed at the waste port; the rest of the stream recirculates up the outer sidewall velocity boundary layer and enters the top Ekman layer. As the gas moves radially inward along the upper Ekman layer, enrichment occurs according to (3.55). For $q < 0$ but $q > q_c$, the stream in the upper Ekman layer meets a stream of gas that rose directly from the feed port and which is also enriched according to (3.59) for $\mathscr{F}_s(a) > 0$. Maximum benefit occurs as $\mathscr{F}_s(a) \to 0+$, so that there is only a slight upward drift in the boundary layer at $r = a$. For $q < q_c$ the effects of differential rotation and/or differential heating exert an increasingly dominant effect on the source–sink flow, and a strong and detrimental net recirculation is set up in the container.

In figure 6, the scaled separation factor $(\alpha - 1)/\{a\epsilon\delta M^2(1 - \omega_E)\}$ is plotted as a function of the cut θ. Note that better enrichment is obtained for smaller values of the cut; this result is compatible with observed centrifuge operation (Olander 1972). Finally, it may be inferred from (3.73) that the enrichment increase is proportional to M^2 for fixed ϵ, θ, a, b and q.

4. Conclusions

In this paper, the mass-transfer problem for a binary gas in a rapidly rotating centrifuge has been formulated and solutions have been obtained for two parameter ranges for a model centrifuge configuration. A practical application to which this

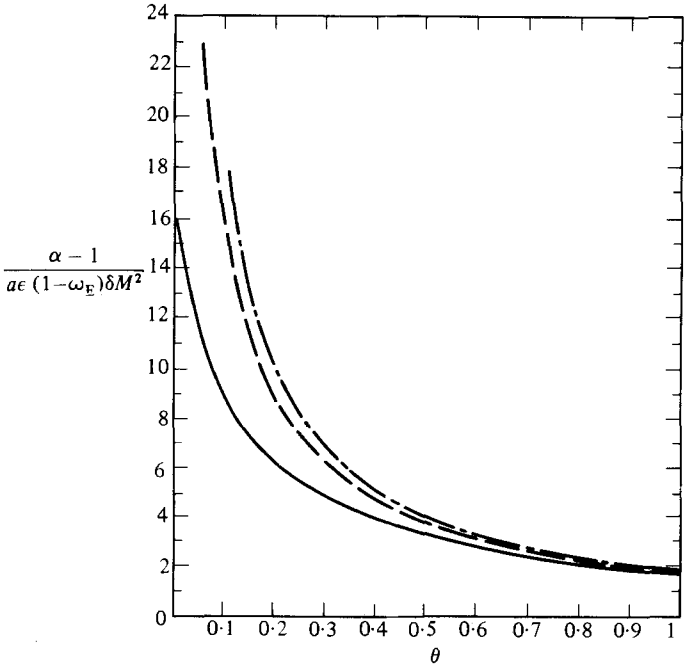

FIGURE 6. Enrichment for small δ versus the cut θ, and $q = -2$ for different values of the rotational Mach Number; ——. $M = 1$; – – –, 2; — — — —, 4.

theory may be applied is the separation of uranium isotopes U_{235} and U_{238}; in this case the working gas is uranium hexafluoride UF_6 (Olander 1972). Solutions for the model centrifuge have been obtained in the two parameter ranges corresponding to moderate and strong forced flow through the centrifuge. In both regimes the results for the separation factor α indicate that: (i) better enrichment is obtained at increased rotational Mach numbers; (ii) enrichment is enhanced for 'fatter' centrifuges corresponding to a smaller inner radius for a given value of the outer radius; and (iii) enrichment decreases with increasing cut. These conclusions are in agreement with observed centrifuge operation (Olander 1972). In the strong-forced-flow case, maximum enrichment occurs for a downward drift in the core of the centrifuge; this drift may be induced either by a differential rotation of end plates (a mechanically driven centrifuge) or by an applied vertical temperature gradient (a thermally driven centrifuge). Increasing enrichment is obtained as the magnitude of the downard drift reaches a critical level where the net vertical motion in the sidewall velocity boundary layers at $r = a$ approaches zero. For geostrophic drift velocities in the core greater than this critical level, a strong recirculation occurs in the container and a depletion of the desirable species occurs at the product port.

Comparison with previous studies of the mass-transfer problem is made difficult because of differences in geometry and differences in the methods of feed and withdrawal. The data of Beams that is used by Nakayama & Torii (1974) in their study of the mass-transfer problem is for a circular cylindrical container. The study of Matsuda (1975) also applies to a cylindrical container where injection and withdrawal occurs through the endwalls. A similar cylindrical geometry is discussed by Soubbaramayer (1979). In general, however, the separation factors computed by these authors are comparable in magnitude to those calculated for the present centrifuge and moreover show the same trends (decreasing enrichment with increasing

feedrates, for example). In addition, it appears that (at least in the early experimental studies) the parameter ranges treated here for $\delta = O(1)$ (moderate forced flow) and $\delta \ll 1$ (strong forced flow) are the practical ranges of interest. Unfortunately, most of the modern experimental work in this area is not available in the open literature and detailed comparison with experiment is not possible here. The trends calculated in this study are qualitatively similar to the numerical results of Nakayama & Torii (1974), Matsuda (1975) and Soubbaramayer (1979); for example, figures 3 and 5 of the present study are qualitatively similar to figure 4.21 of Soubbaramayer (1979).

The analysis described in this paper may be used with some modification to investigate other centrifuge configurations. In particular, work is continuing on the important problem of determining the location of the feed, product and waste ports as well as the cut such that optimal centrifuge performance for a given geometrical configuration may be achieved.

The authors are grateful for helpful discussions with Prof. F. Erdogan.

Appendix

Here the details of the discretization are described for the numerical method used to solve the mass-transfer equation (3.46) subject to the conditions (3.47)–(3.49). A square mesh was defined having a mesh length equal to k in both the r- and z-directions, and standard central-difference approximations were used for each of the derivatives in (3.46); this procedure leads to a difference equation of the form

$$\omega_{i+1,j}\left\{1+\frac{k}{2r_i}\right\}+\omega_{i-1,j}\left\{1-\frac{k}{2r_i}\right\}+\omega_{i,j+1}\left\{1-\frac{k}{2\delta}\rho_{\mathrm{e}}(r_i)\,W_{\mathrm{G}}(r_i)\right\}$$
$$+\omega_{i,j-1}\left\{1+\frac{k}{2\delta}\rho_{\mathrm{e}}(r_i)\,W_{\mathrm{G}}(r_i)\right\}-4\omega_{i,j}=-2k^2. \quad (A\ 1)$$

Here i and j denote typical locations in the mesh in the r- and z-directions respectively, and $0 < i, j < N$, where N is the total number of mesh points in either direction.

The presence of derivatives parallel to the boundaries in both boundary conditions (3.47) and (3.48) requires special consideration. Consider for example the condition (3.48) at $r = a$; it was anticipated that variations in ω normal to the boundaries would be more severe than in the tangential direction and for this reason a sloping-difference approximation was used for the radial derivative, according to

$$k\frac{\partial\omega}{\partial r}\Big|_{r=a,\,z=jk} \approx \tfrac{1}{6}\{-11\omega_{0,j}+18\omega_{1,j}-9\omega_{2,j}+2\omega_{3,j}\}, \quad (A\ 2)$$

where the truncation error is $O(k^4)$ (Abramowitz & Stegun 1965, p. 883; Walker & Dennis 1972). A central difference approximation was made for the z-derivative, and this procedure leads to a difference equation

$$\frac{3}{\delta}\rho_{\mathrm{e}}(a)\,\mathscr{F}_{\mathrm{s}}(a)\{\omega_{0,j+1}-\omega_{0,j-1}\}+11\omega_{0,j}=18\omega_{1,j}-9\omega_{2,j}+2\omega_{3,j}+6ak, \quad (A\ 3)$$

for each internal mesh point ($1 \leqslant j < N$) on $r = a$.

Except at the entrance port, a special treatment of the corner points is required, and as an example consider the mesh modification near the product port at $r = a$, $z = 1$ that is illustrated in figure 7. Here additional mesh points have been introduced

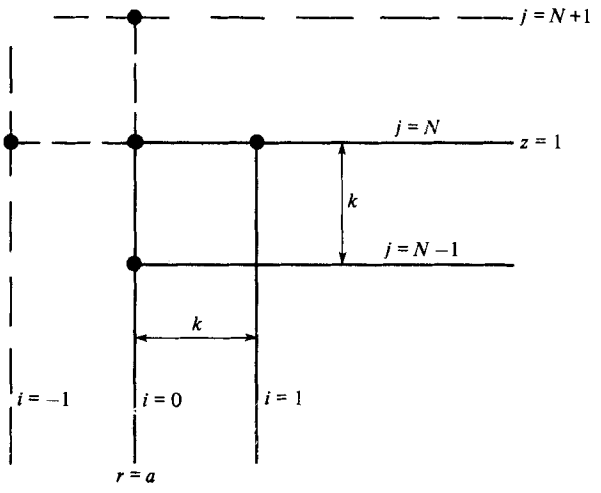

FIGURE 7. Numerical mesh near the product port at $r = a$, $z = 1$. Additional points added to the basic mesh are at the intersection of the broken lines.

outside the container at $(a-k, 1)$ and $(a, 1+k)$. The differential equation (3.46) was approximated at the cornerpoint, and this leads to a finite-difference equation of the form (A 1) with $i = 0$, $j = N$; note that this difference equation involves values of $\omega_{-1,N}$ and $\omega_{0,N+1}$ that are unknown values of ω outside the container. To relate these values to points within the container the boundary conditions (3.47) and (3.48) are applied in the limits $z = 1$, $r \to a$ and $r = a$, $z \to 1$ respectively. Using ordinary central-difference approximations for the derivatives, this procedure leads to

$$-\rho_e(a)\mathscr{F}_{\frac{1}{2}}(a, 1)\{\omega_{1,N}-\omega_{-1,N}\} = \delta\{\omega_{0,N+1}-\omega_{0,N-1}\}, \tag{A 4}$$

$$\rho_e(a)\mathscr{F}_s(a)\{\omega_{0,N+1}-\omega_{0,N-1}\}-\delta ak = \delta\{\omega_{1,N}-\omega_{-1,N}\}. \tag{A 5}$$

These two equations were then used to eliminate the quantities $\omega_{0,N+1}$ and $\omega_{-1,N}$ in (A 1); this technique leads to a single difference equation at the product port involving $\omega_{0,N-1}$, $\omega_{0,N}$, and $\omega_{1,N}$, which is termed the cornerpoint equation. Similar equations were obtained at the corner $r = b$, $z = 1$ and the waste port $r = b$, $z = 0$.

REFERENCES

ABRAMOWITZ, M. & STEGUN, I. A. 1965 *Handbook of Mathematical Functions*. Dover.

BARCILON, V. 1970 *Phys. Fluids* **13**, 537–544.

BARK, F. H. & HULTGREN, L. S. 1979 *J. Fluid Mech.* **95**, 97–118.

BARK, F. H., MEIJER, P. S. & COHEN, H. I. 1978 *Phys. Fluids* **21**, 531–539.

BENNETTS, D. A. & HOCKING, L. M. 1973 *Proc. R. Soc. Lond.* A **333**, 469–489.

BIRD, R. B., STEWART, W. E. & LIGHTFOOT, E. N. 1960 *Transport Phenomena*. Wiley.

BROUWERS, J. J. H. 1976 Doctoral dissertation, de Technische Hogeschool. Twente, Holland.

CONLISK, A. T. 1978 Ph.D. thesis, Purdue University.

CONLISK, A. T. & WALKER, J. D. A. 1981 *Q. J. Mech. Appl. Math.* **34**, 89–109.

HIDE, R. 1968 *J. Fluid Mech.* **32**, 737–764.

HOMSY, G. M. & HUDSON, J. L. 1969 *J. Fluid Mech.* **35**, 33–52.

HULTGREN, L. S., MEIJER, P. S. & BARK, F. H. 1981 *J. Méc.* **20**, 135–157.

LANDAU, L. D. & LIFSHITZ, E. M. 1959 *Fluid Mechanics*. Addison-Wesley.

MATSUDA, T. 1975 *J. Nucl. Sci. Tech.* **12**, 512–518.
MATSUDA, T. & HASHIMOTO, K. 1976 *J. Fluid Mech.* **78**, 337–354.
MATSUDA, T. & HASHIMOTO, K. 1978 *J. Fluid Mech.* **85**, 433–442.
MATSUDA, T., HASHIMOTO, K. & TAKEDA, H. 1976 *J. Fluid Mech.* **73**, 389–399.
MATSUDA, T., SAKURAI, T. & TAKEDA, H. 1975 *J. Fluid Mech.* **67**, 197–208.
MATSUDA, T. & TAKEDA, H. 1978 *J. Fluid Mech.* **85**, 443–457.
NAKAYAMA, W. & TORII, T. 1974 *J. Nucl. Sci. Tech.* **11**, 495–504.
NAKAYAMA, W. & USUI, S. 1974 *J. Nucl. Sci. Tech.* **11**, 242–262.
OLANDER, D. R. 1972 *Adv. Nucl. Sci. Tech.* **6**, 105–174.
ROSSER, J. B. 1968 *Mathematics Research Center, Madison, Wisconsin, T.S.R.* no. 797.
SAKURAI, T. & MATSUDA, T. 1974 *J. Fluid Mech.* **62**, 727–736.
SARMA, S. R. 1975 *Z. angew. Math. Phys.* **26**, 337–345.
SOUBBARAMAYER 1979 Centrifugation. In *Uranium Enrichment* (ed. S. Villani). Springer.
TORII, T. 1977 *J. Nucl. Sci. Tech.* **14**, 901–910.
WALKER, J. D. A. & STEWARTSON, K. 1972 *Z. angew. Math. Phys.* **23**, 745–752.
WOOD, H. G. & MORTON, J. B. 1980 *J. Fluid Mech.* **101**, 1–31.